Chapter

Two-Dimensional Materials for Advanced Solar Cells

Manoj Kumar Singh, Pratik V. Shinde, Pratap Singh and Pawan Kumar Tyagi

Abstract

Inorganic crystalline silicon solar cells account for more than 90% of the market despite a recent surge in research efforts to develop new architectures and materials such as organics and perovskites. The reason why most commercial solar cells are using crystalline silicon as the absorber layer include long-term stability, the abundance of silicone, relatively low manufacturing costs, ability for doping by other elements, and native oxide passivation layer. However, the indirect band gap nature of crystalline silicon makes it a poor light emitter, limiting its solar conversion efficiency. For instance, compared to the extraordinary high light absorption coefficient of perovskites, silicon requires 1000 times more material to absorb the same amount of sunlight. In order to reduce the cost per watt and improve watt per gram utilization of future generations of solar cells, reducing the active absorber thickness is a key design requirement. This is where novel two-dimensional (2d) materials like graphene, MoS_2 come into play because they could lead to thinner, lightweight and flexible solar cells. In this chapter, we aim to follow up on the most important and novel developments that have been recently reported on solar cells. Section-2 is devoted to the properties, synthesis techniques of different 2d materials like graphene, TMDs, and perovskites. In the next section-3, various types of photovoltaic cells, 2d Schottky, 2d homojunction, and 2d heterojunction have been described. Systematic development to enhance the PCE with recent techniques has been discussed in section-4. Also, 2d Ruddlesden-Popper perovskite explained briefly. New developments in the field of the solar cell via upconversion and downconversion processes are illustrated and described in section-5. The next section is dedicated to the recent developments and challenges in the fabrication of 2d photovoltaic cells, additionally with various applications. Finally, we will also address future directions yet to be explored for enhancing the performance of solar cells.

Keywords: 2D materials, graphene, MoS_2, advanced solar cells, perovskites

1. Introduction

Because of excessive utilization and consumption, the conventional fuel sources started depleting rapidly. In this direction, there is an urgent need for reconstruction of energy infrastructure, which is based on environmentally sustainable energy technologies such as wind, water, and solar. The worldwide research attracted towards solar energy, converting light energy into electrical energy. Solar photovoltaic is a pollution-free, efficient, renewable, reliable, rich, and continual source of energy. The photovoltaic solar cell, well-known technique, provides the solution

of energy source crises in the 21st century. The main mechanism for the conversion of light to electricity: photovoltaic effect, photoconductivity, and photovoltaic effect (bulk). There is the requirement of a p-n junction in which electron and holes (photo-induced) in p-type and n-type materials partitioned transport a gathered to an electrode for production of photocurrent. In 1839, Edmond Becquerel first of all showed the demonstration of photovoltaic effect [1–2]. In the absence of p-n junction the conductivity of the semiconductor sample rises (by the illumination), it happens when the number of free electrons is increased, this is famed as photoconductivity. The electricity generated through the photovoltaic solar cells is not so cost-efficient in comparison to the grid power which we are using today [3]. At the large scale the solar energy conversion which should be low cost, there is a need for such type semiconducting materials that will make the production processes easily measurable and economically feasible [4]. In this direction two-dimensional (2d) material is referred to as impediment in one dimension between the size range 0–100 nanometers (nm), while the rest of the two dimensions are of micrometer range [5]. Furthermore, the configuration of atom and bond strength in 2d is identic and much stronger than that of bulk materials [6]. Also, ultrathin 2d nanomaterials have uncommon properties from their alternative nanostructured materials, such as three-dimensional (3d) nanocubes, one-dimensional (1d) nanotubes, and zero-dimensional (0d) quantum dots. First, the ultra-thickness of 2d nanomaterials provides high charge carrier, high charge mobility both at low and 300 kelvin (K) temperature, and high thermal conductivity [7–9]. Second, quantum confinement of 2d nanomaterials especially single layer or atomic thick layer, displays a number of properties, such as conductivity, tunable bandgap, surface activity, and magnetic anisotropy [10–11]. Third, the quantum Hall Effect (QHE) is shown by defect-free 2d materials, even at 300 K. The defect-free 2d materials have the electrons with a concentric (scatter-less) motion that allows the high charge carrier [12–13]. Fourth, the large ultrahigh surface area, keeping atomic-sized thickness, shows them ultrahigh specific surface area [14–15]. Therefore, photovoltaic solar cell manufactured by two-dimensional materials is a well-versed method in between of scientific community.

In the present chapter, we aim to follow up on the most important and novel developments that have been recently reported on solar cells. Section-2 is devoted to the properties, synthesis techniques of different 2d materials like graphene, transition metal dichalcogenides (TMDs), and perovskites. In the next section-3, various types of photovoltaic cells, 2d Schottky, 2d homojunction, and 2d heterojunction have been described. Systematic development to enhance the power conversion efficiency (PCE) with recent techniques has been discussed in section-4. Also, 2d Ruddlesden-Popper perovskite explained briefly. New developments in the field of the solar cell via upconversion and downconversion processes are illustrated and described in section-5. The next section is dedicated to the recent developments and challenges in the fabrication of 2d photovoltaic cells, additionally with various applications. Finally, we will also address future directions yet to be explored for enhancing the performance of solar cells.

2. Photovoltaic materials

2.1 Graphene

The dimension is the key factor to classify carbon allotropes/nanostructures into four groups, 0d (quantum dots, fullerenes), 1d (nanohorns, nanoribbons,

carbon nanotubes), 2d (graphene) and 3d (diamond, graphite) structures [16–17]. A new area of research started with the groundbreaking discovery of graphene in 2004 by Novoselov and his co-authors in his famous publication "Electric field effect in atomically thin carbon films" and awarded jointly Nobel prize for it [18]. Graphene is a single layer structure with sp^2 hybridization in which carbon atoms are arranged in a hexagonal honeycomb lattice. It is a semimetal with zero-bandgap, large specific surface area (2630 m^2g^{-1}), high Young's modulus (1.1 TPa), and high thermal conductivity (3×10^3 W m^{-1} K^{-1} at 300 K) [6, 19–22]. Graphene also provides the optical and electrical properties as excellent transparency (97.7% in the visible spectrum) and electrical conductivity ($\approx 10^4$ Ω^{-1} cm^{-1}) [23–24]. These exotic properties of graphene make it special in several optoelectronic applications. In solar cells, instead of indium doped tin oxide (ITO) and fluorine-doped tin oxide (FTO), graphene attracted attention due to flexibility, chemical stability, and high transmittance [20, 25–26]. These excellent dimensional, structural, optical, and electrical properties depict the graphene as a suitable aspirant for photovoltaic cells.

One of the well-known methods to synthesis the graphene is thermal chemical vapor deposition. In the thermal chemical vapor deposition (CVD), copper substrate placed into the quartz tube and then precursor gases (in the specific ratio) are allowed to flow at very high temperatures in the furnace [27]. After some time, single layer, bilayer, or multilayer deposition of graphene revels, this depends upon the internal conditions of experiments like temperature, pressure, reaction time, and gas flow rate [28]. The more advancement in the synthesis of graphene on Ni was achieved by Somani *et al*. [29]. In this, the camphor ($C_{10}H_{16}O$) has been taken as the precursor. Moreover, the large-scale monolayer graphene was produced by Obraztsov and co-others via a CVD method [30]. Another attempt has been performed to manufacture graphene on Cu foil (industrial base) via thermal CVD of methane with 1000°C temperature by Lia and co-workers in 2009 [31].

2.2 Transition metal dichalcogenides

Although graphene has various excellent properties, due to zero-bandgap, work-function, and toxic nature, the research on new atomically thin 2d materials gained attention. These necessities have been fulfilled by TMDs. These2d materials attracted more attention as they have grown on a flexible surface and can be bears the stress and deformation [32–34]. Generally, TMDs are formulized as $MX_2$where M expresses the transition metal from group IV-VIII, (M = Ti, Zr, Hf, V, Nb, Cr Ta, Mo, W, etc.) and X is a chalcogen atom (X = S, Se, Te) [35–36]. TMDs have opened the new pipeline of research as having tunable bandgap (1–2 eV) and explore an excellent picture of electrical, optical, and mechanical properties [37–39]. Various combinations of TMDs such as MoS_2, CrS_2, WS_2, TiS_2, $MoSe_2$, $CrSe_2$, WSe_2, $TiSe_2$ etc. found in metallic, semiconductor and insulator phase [40]. TMDs are a collection of big crystal family, found in different phases such as 1 T, 2H, and 3R., having two-third materials with layered structure [41]. In particular, MoS_2 shows mechanically 30% more strength than steel and can be ruptured after warping 1%. It generates the most distensible and strongest semiconducting materials [36, 42]. Counter electrodes manufactured by platinum (Pt) were replaced by MoS_2 in photovoltaic devices [43].

Typically, the synthesis approaches like exfoliation, hydrothermal, CVD, molecular beam epitaxy (MBE), and atomic layer deposition (ALD) are used to prepare the desired size of TMDs [44–48].

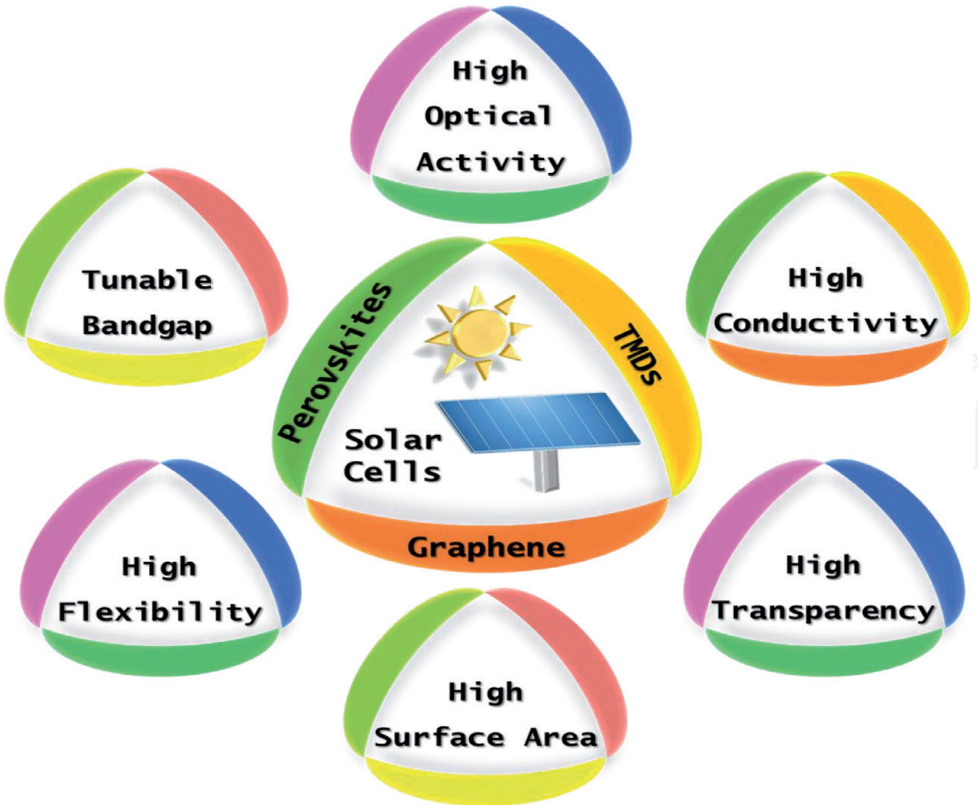

Figure 1.
Schematic illustration of exotic properties of 2d materials used for solar cell devices.

2.3 Perovskites

Perovskites are a mixture of organic–inorganic materials, which offer high absorption coefficients, direct bandgap, high charge carrier mobility, and long charge carrier diffusion length [49–50]. This is why the research groups attracted more and more attention by 2d perovskites for a long time. There are three types of halide perovskite (2d) (i) organic–inorganic mixed halide perovskite, (ii) 2d Ruddlesden-Popper perovskites, (iii) inorganic halide perovskite [51]. The typically Perovskite structure is given by ABX_3, where A indicates monovalent cation such as methyl rubidium (Rb), ammonium, and formamidinium; B represents heavy materials like tin (Sn) and lead (Pb); and X shows a halogen anion (i. e. chlorine, bromine, iodine). A unique type of properties provides highly defected bulk structures, indicate chemical compound through which the device operation power has been smoothed. The performance of 2d perovskite solar cells can be improved by obtaining a very high output voltage (under the circumstance of open circuit V_{oc}). The photovoltaic solar cells should be free from all recombination losses and this can be achieved by suppressing losses up to unity while quantum yield must be highest. [52–53].

The synthesis of 2d organic–inorganic mixed halide perovskite fabricated in two steps: (i) formation of lead halide (nano-platelets) on muscovite mica using van der Waals epitaxy in vapor transport CVD system, (ii) Ag as-solid heterophase reaction (using methylammonium halide molecules) used to obtain perovskite from platelets. However, the structure fabricated via this method is a 3d perovskite but using the universal scotch tape-based mechanical exfoliation method 2d perovskites is obtained [54–57]. **Figure 1** shows schematic illustration of exotic properties of 2d materials useful for solar cell devices.

3. Photovoltaic in domain of 2d materials

3.1 Photovoltaic based on 2d Schottky junction

During the photovoltaic processes (under illumination), electron–hole pairs are formed. These pairs are also termed as photogenerated carriers and they can be equal and more energetic (with incident photons) by the bandgap of the semiconductor. The conjunction of electron–hole pairs accorded on the electrodes and they are isolated through the junction internal field (electric) [58]. When the difference between the Fermi level of semiconductor and metal work function is generated, a Schottky junction enters in the pictures and photocurrent starts to develop. Net photocurrent has been maintained in asymmetric Schottky barriers (metal having different work function), whereas symmetric metal contact structure produces no net photocurrent. The important characteristics terms associated with the photovoltaic device illustrated in **Table 1**. Fontana *et al.* [58] synthesized a MoS_2 based (50 nm thick) phototransistor with palladium (Pd) and gold (Au) for drain contact and source, respectively. When two different materials are used for the source and drain contacts, such as hole-doping Pd and electron-doping Au, the Schottky junctions formed at the MoS_2 contacts generates a photovoltaic effect. **Figure 2a** displays the optical image of the device. **Figure 2b** shows the current vs. voltage curve at zero gate voltage, corresponding to the branch of the hysteresis with higher current, where the Fermi energy is shifted into the MoS_2 conduction band. Shin *et al.* [59] reported the graphene/porous silicon Schottky-junction solar cells by employing graphene transparent conductive electrodes doped with silver nanowires. The Ag nanowires-doped graphene/PSi solar cells show a maximum PCE of 4.03%. Yi and his co-workers developed Schottky junction photovoltaic cells based on multilayer $Mo_{1-x}W_xSe_2$ with x = 0, 0.5, and 1 [60]. To generate built-in potentials, Pd and Al were used as the source and drain electrodes in a lateral structure, while Pd and graphene were used as the bottom and top electrodes in a vertical structure.

3.2 Photovoltaic based on 2d homojunction

Due to the very low efficiency of the Schottky junction, more research efforts are required to improve photovoltaic processes in the semiconducting p-n junction.

Term	Description
Short-circuit current (I_{sc})	It is defined as the current flowing through the device (under illumination) and at zero external bias having contact shorted.
Power conversion efficiency (PCE)	It is defined as the ratio of electrical power generated to the incident light power.
External quantum efficiency (EQE)	The ratio defines by the amount of charge carriers moving through the device (under short-circuit current) to the all number of colliding photons on it.
Internal quantum efficiency (IQE)	Shows the ratio of the amount of charge carriers moving through the device (under short-circuit current) to all numbers of absorbed photons.
Open-circuit voltage (V_{oc})	The voltage produced by the device having no current flow (under illumination)
Fill factor (FF)	It is describing the ratio of maximum electric power generated to the product of its open-circuit voltages and its short-circuit current.

Table 1.
Main terms to demonstrate the photovoltaic device.

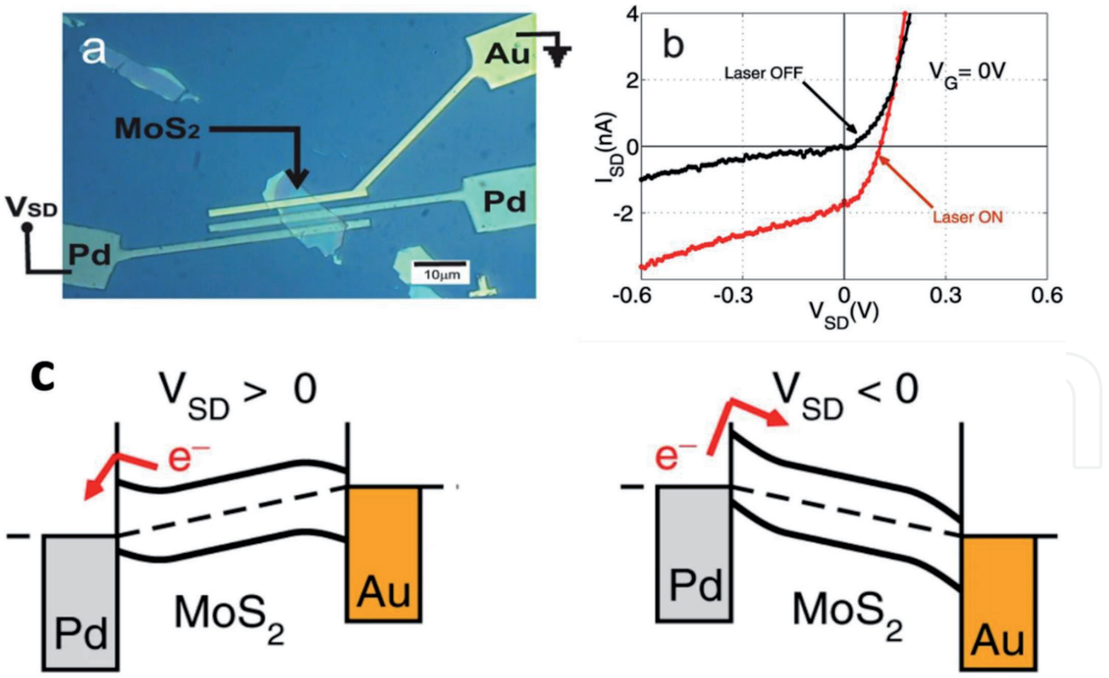

Figure 2.
Photovoltaic effect with Pd-Au bias configuration. (a) Optical image of the device. The spacing between the electrodes is 2 μm. (b) Current vs. source-drain voltage (at V_G = 0) showing strong asymmetry and photoresponse with diode-like behavior for the Pd-Au bias configuration indicated in (a). (c) Effect of source-drain bias on a device with one Au and one Pd electrode. Reprinted with permission from [58]. Copyright (2013) springer nature.

Using a splitting gate on monolayer WSe_2, Pospischil *et al.* [61], Baugher *et al.* [62], and Ross *et al.* [63] effectuated experimentally p-n junctions. This demonstration of WSe_2 monolayer flake has been achieved with mechanical exfoliation after that shifted onto a pair of split gates slipover with previously formed gate dielectric materials (SiN, HfO_2). The charge density and the conduction type (into the monolayer thick channel) can be modulated by electrostatic control after dissimilar voltages have been applied on the two local gates and the automatically thin p-n junction was formed. Due to this remarkable rectification in the diode behavior occur, finally able to photovoltaic generation. Taking the gap within two gates as a photoactive area the power conversion of 0.5% was demonstrated by Pospischil *et al.* with V_{oc} of 0.64 V and illumination of 140 mW/cm^2 (halogen source). The remarkable results are in the picture with very high efficiency of photovoltaic energy conversion, assuming the monolayer WSe_2 (95% transparency), which opens a pipeline of single-layer TMDs for semi-transparent solar cells. Memaran *et al.* [64] successfully demonstrated the composition of electrostatically generated $MoSe_2$ multilayer p-n junction to achieve high photovoltaic performance.

In addition to modifying the photovoltaic parameters, the 2d black phosphorous (BP) has attracted more attention of researchers due to its remarkable optical and electrical properties, keeping in mind its unique bandgap (≈0.3–2.0 eV), in-plane anisotropy and high carrier mobility i.e. 1000 cm^2/Vs, hence BP shows the possibility for broadband optoelectronic applications [65–67]. Choi *et al.* [68] develop a technique to form a lateral homogeneous 2d MoS_2 p-n junction by partially stacking 2d h-BN as a mask to p-dope MoS_2. The fabricated lateral MoS_2 p-n junction with asymmetric electrodes of Pd and Cr/Au displayed a highly efficient photo response such as maximum external quantum efficiency of ~7000%, specific directivity of ~5 x10^{10} Jones, and light switching ratio of ~10^3. **Figure 3** shows the fabrication of the MoS_2 p-n diode. **Figure 3b** shows the optical microscopy image of MoS_2 p-n diode with hetero electrodes.

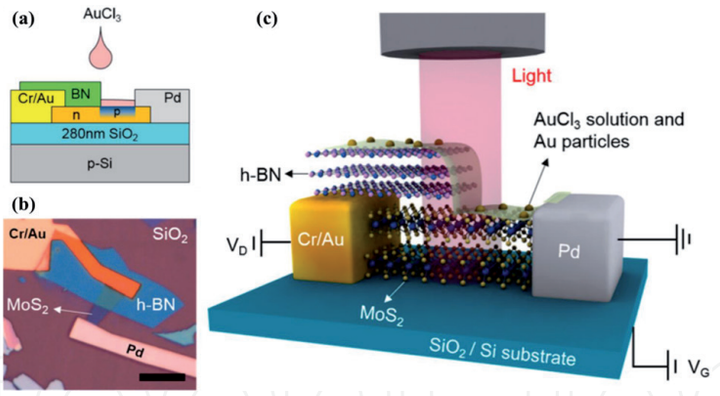

Figure 3.
Fabrication of the MoS_2 p-n diode. (a) Cross-sectional diagram and (b) optical microscopy image of MoS_2 p-n diode with hetero electrodes. The scale bar indicates 10 μm. (c) Three-dimensional schematic and circuit diagrams of the fabricated MoS_2 p-n diodes under light illumination. Reprinted with permission from [68]. Copyright (2014) American Chemical Society.

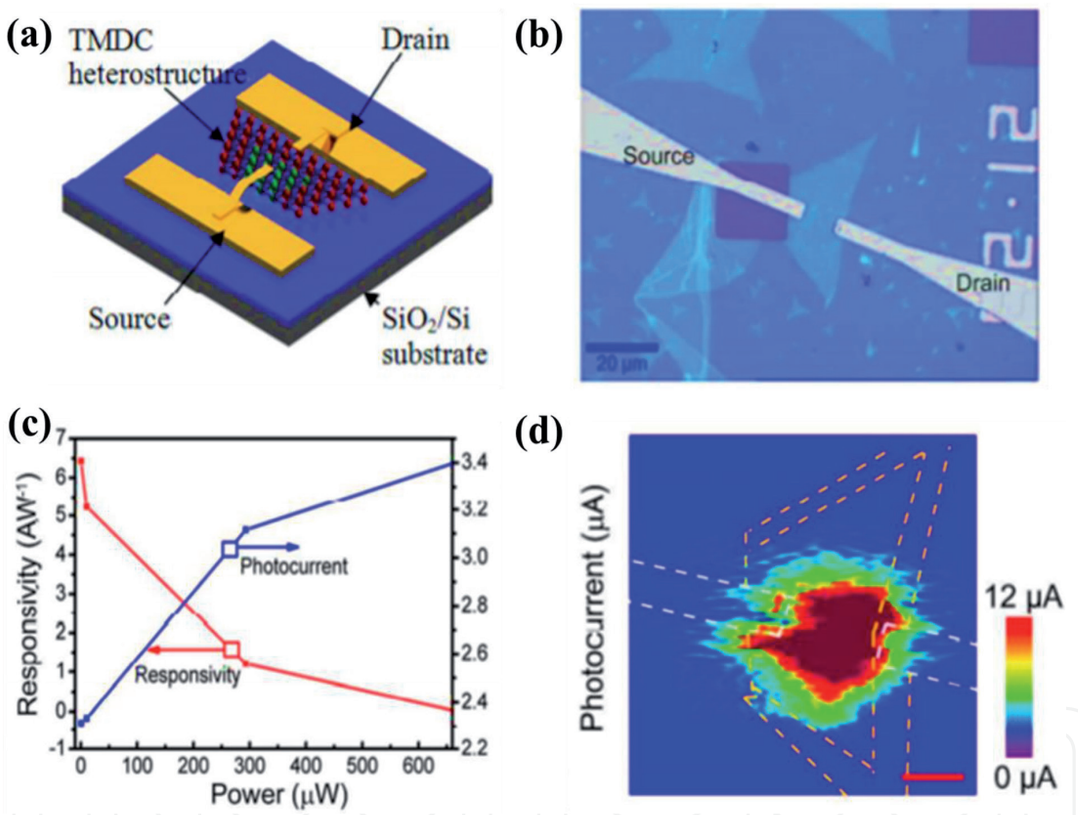

Figure 4.
(a) Schematic diagram of the photodiode based on the WSe_2/WS_2 heterojunction. (b) Optical image of the photodiode device. (c) Photocurrent and responsivity as a function of the incident power. d) the photocurrent image is taken from the device in (b). Reprinted with permission from [71]. Copyright (2017) American Chemical Society.

3.3 Photovoltaic based on 2d heterojunction

The p-n heterojunctions work as a basic backbone of various optoelectronic devices and applications due to various theoretical and experimental restrictions, there is the need for manufacturing designed heterostructures. Duan *et al.* [69] demonstrate the modulated MoS_2-$MoSe_2$ and WS_2-WSe_2 lateral heterostructures by thermal chemical vapor deposition (CVD) technique. The well-known n-type (WS_2) and p-type (WSe_2) builds natured heterojunction p-n diode with current rectification. When such heterojunction p-n diodes are characterized. The

photovoltaic effect with a V_{oc} of ≈ 0.47 V and I_{sc} of ≈1.2 nA was established with laser illumination conditions (514 nm and 30nW). The internal quantum efficiency (IQE) and external quantum efficiency (EQE) were found to be 43% and 9.9% respectively The active regime was selected as lightly doped WS_2 and WS_2-WSe_2 interface region through photocurrent mapping, implies with the fact "A large fraction of the depletion layer is localized to the lightly doped WS_2 of the diode" [69]. Atomically sharp in-plane WSe_2/MoS_2 interface automatically comes into the picture with a high-magnification scanning transmission electron microscope (STEM), these force the photovoltaic effect of the intrinsic single layer p-n heterojunction was indorsed [70]. Li *et al.* [71] successfully fabricated a composition graded doped lateralWSe_2/WS_2 heterostructure by ambient pressure CVD in a single heat-cycle. The optoelectronic device (**Figure 4a-b**) based on the lateral WSe_2/WS_2 heterostructure shows improved photodetection performance in terms of a reasonable responsivity and a large photoactive area. The photocurrent and photo-responsivity are also depicted in **Figure 4c**. The photocurrent appears to increase nonlinearly, whereas the photoresponsivity decreases as the light power increases, with the highest obtained photoresponsivity of 6.5 $A.W^{-1}$. The reduction of the photoresponsivity at higher light powers may be ascribed to the reduction of unoccupied states in the conduction bands of WSe_2 and WS_2.

4. Perovskite 2d materials for photovoltaic cells

4.1 Transport layers in regular (n-i-p) photovoltaic

The layer-by-layer deposition technique is used to manufacture photovoltaic solar cell devices (PSCs). In these types of constructions, the order of charge selective layers in the manner can prosecute subdivide the devise configuration in two ways, regular PSCs (n-i-p) and inverted PSCs (p-i-n). The PSCs have two parts, (a) metal contact, (b) transparent conductive glass (TCO), while a slice of the observer has been arranged between hole transporting layer (HTL) and electron transporting layer (ETL). When the perovskite absorbs the light, an exciton i. e. the carriers are partitioned and moved towards the adequate layer, HTL, and ETL. Hence the charge carriers are shifted to the different electrodes. Moreover, ETL and HTL are performing two main roles, control the perovskite crystal growth, and extract and move the charge carriers. It is well versed that the hysteresis phenomenon is chiefly linked with the characteristics and interface of the charge selective layers to the perovskite [72–73]. Some of the remarkable features of ideal ETL and HTL materials are high transparency, high charge mobility, inherent stability, low-cost manufacturing, and appropriate energy alignment.

2,2,7,7-tetrakis (N,Npdimethoxyphenylamino)-9,9-spirobifluorene (Spiro-OMeTAD) and TiO_2 are the wall known materials that can be used as hole transport material (HTM) and electron transport material (ETM) respectively in the formation of n-i-p PSCs. On the other hand poly(3,4 ethylenedioxythiophene)–polystyrene sulfonate (PEDOT:PSS) and fullerene derivatives (e.g., 6,6-phenyl-C61-butyric acid methyl ester (PCBM)) has been taken as the HTM and ETM to manufactured the p-i-n PSCs [74–76]. Singh *et al.* [77] described the direct synthesis of MoS_2 (transparent, thin, and uniform) films on FTO- coated glass by the use of microwave irradiation and utilize this ETL in perovskite solar cells. TiO_2-coated FTO, SnO_2, MoS_2, and FTO-only substrates were prepared and their photovoltaic performances were checked and they have maximum PCEs with 17.15%, 15.80%, 13.14%, and 6.11% respectively [77]. When the article examination of the lifetime of charge

carriers and charge recombination dynamics of ETL/Perovskite seems to be MoS_2 as shortest charge carrier lifetime as with other ETLs, which shows the charge extraction.

Yin *et al.* [78] reported the PCE of 17.37% by taking TiS_2 nanosheets (8–9 layers) suspended in isopropanol alcohol (IPA) in the perovskite solar cells. Uniquely, encapsulated perovskite solar cells with TiS_2 ETL demonstrate the highest stable under the conditions (UV irradiation 10 mW cm^{-2} and in ambient atmosphere for 50 h), with the result of 90% PCE. A double of SnO_2 and 2d TiS_2 synchronously, used for the PCE of 21.73% performed by Huang *et al.*, as every potential ETLs [79].

Applying the self-assembly stacking deposition method, the PCE of SnS_2 ETL based device, up to 20.12% has reported by Zhao *et al.* [80]. The Ti_3C_2 integration into a SnO_2 ETL for low-temperature planer perovskite solar cells by Yang and his co-workers by varying the loading of MXene from 0 to 2.5 wt% [81]. The device formed has the value of PCEs modified from the value of 17.23% to 18.34% at 1 wt% (increasing the loading of MXene). In the addition, the device fabricated through a SnO_2-$Ti_3C_2$is highly stable (with, RH-20%), and shows the PCE up to 80% of their initial performance after 700 h (identical with SnO_2-only devices) [81].

To increase the charge transfer efficiency, the perovskite crystal size, and lower the defect density, Guo *et al.* [82] explained $Ti_3C_2T_X$ MXene as an external material for the perovskite precursor solution. The results reveal that the incorporated device experimentally verified a PCE of 17.41% with short-circuit current (J_{SC}) of 22.26 mA cm^{-1} which is comparably high with the pristine perovskite device having the PCE of 15.54% and J_{SC} of 20.67 mA cm^{-1}.

Wang and his research group [83] experimentally verified that whenever a tiny amount of black phosphorus added to the $MAPbI_3$ starting solution (precursor), the photostability and efficiency of perovskite solar cells have been critically enhanced. The few-layer black phosphorus is proved to obtain ample perovskite to the size greater than 500 nm with the comparison bare $MAPbI_3$ film size (<400 nm). Taking the complex structure FTO/c-TiO_2/SnO_2/perovskite/Spiro-OMeTAD/Ag and $MAPbI_3$/BP for PSCs, the unique PCE of 20.65% was achieved, having less hysteresis and high reproducibility. Under the continuous white light-emitting diode (illumination of 100 mW cm^{-2} within the N_2 glove box) the $MAPbI_3$/BP-based PSCs show an excellent PCE limit of 94% (1000 h) [83–84].

The spiro-OMeTAD HTL and perovskite on active buffer layer (liquid phase exfoliated few-layer MoS_2 nanosheets) instead by Cappaso and co-workers and tried to solve the problem [85]. The above arrangement completes two necessary conditions i.e. prominent layer to ease the injection process and hole collection and performing like a barrier so that metal electrode migration can be curbed. The N-methyl-2-pyrrolidone solvent is very famous for the experimentalist to efficient MoS_2 [86–87]. On the other hand, some study proves this solvent not suitable for perovskite, to make it perovskite favorable solvent (IPA), a solvent exchange process has to be required.

Najaf*et al.* [88] developed "graphene interface engineering" strategy based on van der Waals MoS_2 QD/graphene hybrids that enable $MAPbI_3$-based PSCs to achieve a PCE up to 20.12% (average PCE of 18.8%).The van der Waals hybridization of MoS_2 quantum dots (QDs) with functionalized reduced graphene oxide (f-RGO), obtained by chemical silanization induced linkage between RGO and (3-mercaptopropyl)trimethoxysilane. This results in homogenize the deposition of the hole transport layer (HTL) or active buffer layer (ABL) onto the perovskite film since the two-dimensional nature of RGO effectively plugs the pinholes of theMoS_2 QD films. **Figure 5a** represents the sketch of mesoscopic $MAPbI_3$-based PSC exploiting MoS_2 QDs:f-RGO hybrids as both HTL and ABL. The normalized

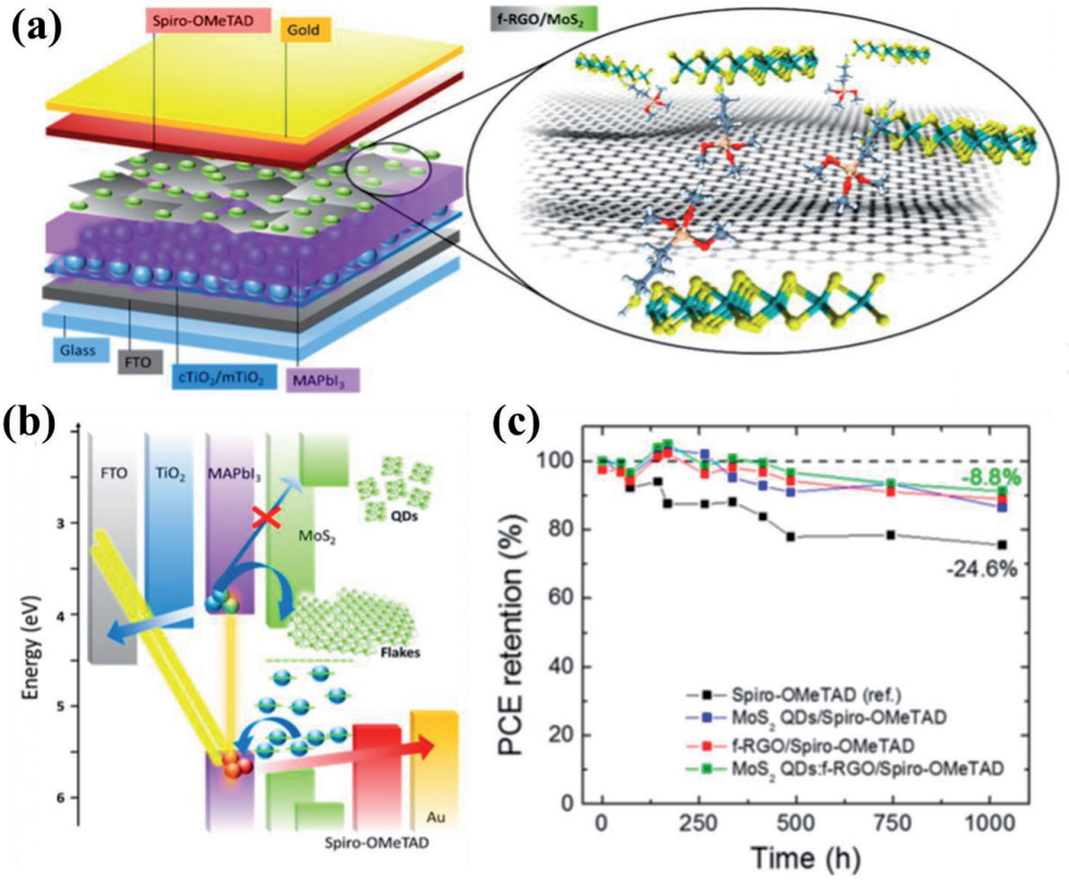

Figure 5.
(a) Sketch of mesoscopic $MAPbI_3$-based PSC exploiting MoS_2 QDs:f-RGO hybrids as both HTL and ABL. (b) Scheme of the energy band edge positions of the materials used in the different components of the assembled mesoscopic $MAPbI_3$-based PSC. (c) Normalized PCE trends vs. time extracted by I – V characteristics under 1 sun illumination. Reprinted with permission from [88]. Copyright (2018) American Chemical Society.

PCE trends vs. time extracted by I – V characteristics under 1 SUN illumination, periodically acquired during the shelf life test (ISOS-D-1), shows in **Figure 5c**.

4.2 Transport layers in inverted (p-i-n) photovoltaic

The organic solar cell is the key to fabricate the p-i-n PSC structures [89]. Huang *et al.* [90] successfully showed that with coverage optimization, a planar p-i-n^{++} device with a PCE of over 11% was achieved. This also suggests that the ETL may not be necessary for an efficient device as long as the perovskite coverage is approaching 100%. **Figure 6a-b** presents the device architecture of the perovskite solar cells with (a) and without (b) a TiO_2 ETL. **Figure 6c** shows the current density-voltage curves of two typical $CH_3NH_3PbI_{3-x}Cl_x$-based solar cells grown on FTO substrates with and without UVO treatment under simulated AM1.5G solar irradiation (100 mW/cm^2). Jeng and co-workers reported that perovskites have the ability to transport the holes [91]. To achieve a PCE of 15.1%, Hu *et al.* proposed a surface-modification technique in which the ITO surface/optimize energy level by using the cesium salt solution [92].

Liu and his co-workers reported layer free PSC with an efficiency of 13.5% to obtain this, perovskite layer directly put together with the ITO surface by using a sequential layer deposition method. The above arrangement proves that to enhance device efficiency ETL is not required always [93]. Ke *et al.* [94] manufactured ETL free PSC with efficiency 14.14% and V_{oc} 1.4 V deposited directly on FTO substrate (via a one-step solution process) in which no hole blocking layers

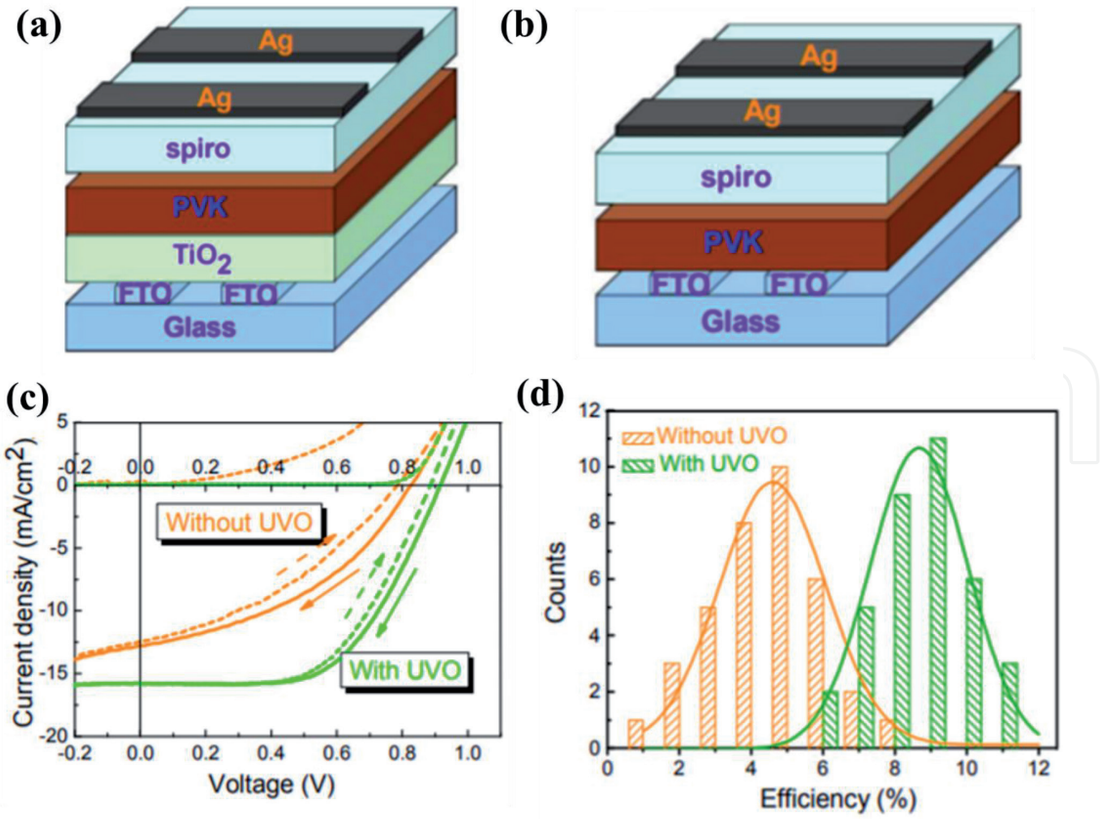

Figure 6.
Device architecture of the perovskite solar cells (a) with TiO_2 ETL and (b) without TiO_2 ETL (c) J-V curves of $CH_3NH_3PbI_{3-x}Cl_x$-based solar cells with and without UVO treatment (d) histograms of their corresponding PCE values measured for 36 separate devices (c). Reprinted with permission from [90]. Copyright (2016) American Chemical Society.

are required. He further described that TiO_2 (electron-transporting material) is not a perfect interfacial material. It is also described Liu *et al.* [93], Chen *et al.* [95], and Prochowicz *et al.* [96] that the efficiency of compact layer-free devices can be higher when various film-forming techniques are to be used.

Various quantities of black phosphorus quantum dots (BPQDs) mixed with $MAPbI_3$ precursor solution to form p-i-n inverted devices [97]. These BPQDs based perovskite films revealed less non-reactive defects, larger grain size, and higher crystallinity, with a comparison of no BPQDs perovskite films. Further, it is clear from some experimental facts that BPQDs also work as heterogeneous nucleation sites. This leads to the growth of perovskite crystals with homogeneity. The PCE of 20% was obtained for additive-assisted perovskite film. Adding the BPQDs on the lower surface of $MAPbI_3$-the enhanced crystalline of $MAPbI_3$-BPQDs film has been achieved.

4.3 2d Ruddlesden-popper perovskite

The hybrid organic–inorganic halide perovskite (OIHPs) are very unsuitable in the industrial fabrication of solar device as they lose the stability on heating, moisture, and light. These major issues have been resolved by S. N. Ruddlesden and P. Popper to fabricate the perfect candidates known as Ruddlesden-Popper perovskite (RPPS). This is the mixture of 2D/3D materials and can be used in LEDs as it has an intense photoluminescence feature [98]. The 2D Ruddlesden-Popper (2DRP) perovskites are the topic of great interest and research because highly stable PSCs can be fabricated by them [99]. The general form of 2DRP is $(A')_2\,(A)_{n-1}B_n\,X_{3n+1}$, where A' indicates $R\text{-}NH_3$ or $H_3N\text{-}R$ (R an aromatic ligand or large aliphatic alkyl chain) and works as an insulating layer to partitioned the various inorganic layers. A describes small cation

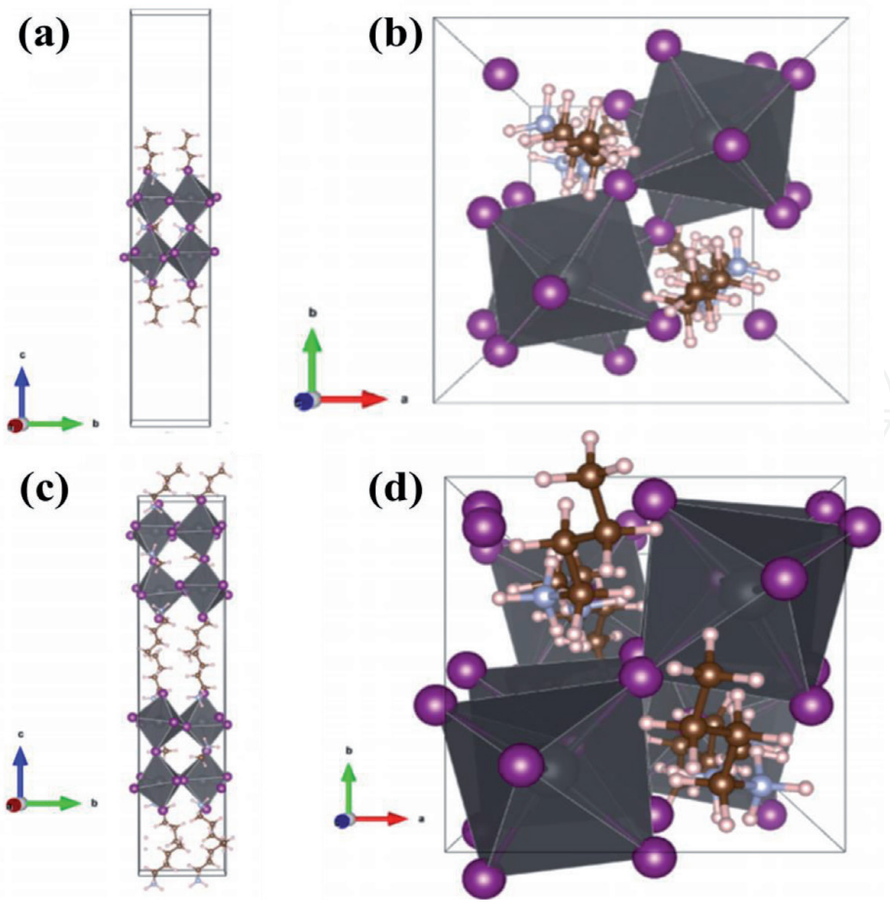

Figure 7.
(a) Lateral view and (b) top view of the n = 2 sheet (NS-RPP) optimized structure. Same (c, d) for the bulk QW (QW-RPP). [gray: Pb; purple: I; Brown: C; light blue: N; white: H atoms]. Reprinted with permission from [98]. Copyright (2018) American Chemical Society.

such as $CH_3NH_3^+$ and Cs^+. B represents Pb^{2+} and Sn^{2+}, divalent metal cation, while X describes the halides. Various values of small n provide us strict 2D structure (n = 1), quasi-2D structure (n = 2–5), conventional 3D structure (n = ∞), and represents the number of metal halide, monolayer sheets [100]. These 2DRP excellently perform thermal stability, humidity stability, and structure stability [101–106]. Giorgi *et al.* [98] showed a lateral and top view of the nanosheets Ruddlesden–Popper organic–inorganic halide perovskites (NS-RPPs) optimized structure in **Figure 7a-b**. Also, lateral and top view of the quantum-well Ruddlesden–Popper organic–inorganic halide perovskites (QW-RPPs) structures in **Figure 7c-d**. The solution base synthesis, colloidal base method, liquid, and vapor-based epitaxy, exfoliation method, and single crystal growth are the well-known growing technique to fabricate 2DRP perovskites [107]. Niu *et al.* [108] prepared mono and few layers $(C_6H_9C_2H_4NH_3)_2$ PbI_4 flakes via the method of micromechanical exfoliation.

5. Conversion treatment for photovoltaic cells

5.1 Downconversion of perovskite photovoltaic cell

In the previous investigations, various techniques and methods have been adopted to improve the efficiency of solar cells, higher by the Shockley and Queisser limit (32%). The phenomenon of splitting, low energy photons by high energy photons (single) is known as downconversion (quantum cutting). An ample work has been done on downconversion for photovoltaic devices. This was performed

with lanthanide ions because of its excellent optical properties. Various experiments also proved the use of nanomaterials as down converters. If we chose the lanthanide ions and design of the solar cell, there will be a maximum benefit to using the down-conversion materials. The host materials should possess properties like low scattering, absorption strength, thermal and chemical strength, high transmittance, photo-stability, and excitation energy [109–110]. The necessary conditions to pick the lanthanide ion are good electrical and chemical stability and high emission lifetime. Downconversion Tb^{3+}-Yb^{3+} has also been demonstrated in $GdAl_3(BO_3)_4$ [111], $GdBO_3$ [112], Y_2O_3 [113], CaF_2 nanocrystals [114] and lanthanum borogermanate glass [115]. Tsai *et al.* [116] explored the graphene quantum dots (GQDs) as a down conversion in then-type Si heterojunction (SHJ) solar cells.

The photographic image and the cross-sectional schematic of the SHJ solar cell are shown in **Figure 8a-b**, respectively. **Figure 8c-d** shows the low-magnification and high-magnification top-view SEM images of the micro pyramids of SHJ solar cells. The device with 0.3 wt % of GQDs shows the highest short-circuit current (J_{SC}) and fill factor (FF) of 37.47 mA/cm^2 and 72.51%, respectively, which leads to the highest PCE of 16.55% (**Figure 8f**). The external quantum efficiency (EQE) of the devices with 0.3 wt % and without GQDs and the EQE enhancement are shown in **Figure 8g**. The efficiency enhancement is due to the photon down conversion phenomenon of GQDs to make more photons absorbed in the depletion region for effective carrier separation, leading to the enhanced photovoltaic effect. Various down conversion materials were described and synthesized to enhance UV stability and UV photon harvesting [117–118].

5.2 Upconversion of perovskite photovoltaic cell

The conversion (nonlinear optical process) in which minimum two low energy photons, present in the near-infrared region into high energy photon with the visible region known as upconversion [119–120]. The upconversion materials contain large bandgap, seem to be most favorable for solar cell applications. Various uses of upconversion materials are optical data storage, medical therapy, display technology, light-harvesting, temperature sensors, and solid-state lighting. Trupke *et al.* [121] theoretically investigated that if a perfect upconvertor is used with conventional single-junction bifacial solar cells (bandgap 2 eV), we can obtain PCE of 47.6% (non-concentrated sunlight) and 63.2% concentrated sunlight. Lanthanide based upconverters and organic upconverters are very common to improve the efficiency of photovoltaic devices. The elements lanthanum to lutetium are used as the upconverters. In addition, enhancement in the photocurrent has been achieved by the use of two commercial upconverters on both sides of Si solar cells (Pan *et al.*) [122].

The nano precursor upconversion materials Er^{3+}/Yb^{3+} co-doped with TiO_2 and LaF_3 have been explored by Shan *et al.* [123]. Shang *et al*. [124] also explored the various techniques to enhance efficiency via upconversion. The utilization of light beyond the visible region is not possible by PSCs ($CH_3NH_3PBI_3$), due to their intrinsic bandgap. The upconversion is a specific way, to harvest this regime and convert it in the visible regime, so that the PSCs IR response can be increased. Chen and co-workers reported that the efficiency will be increased if $LiYF_4$: Yb^{3+}, Er^{3+} single-crystal attached in the front part of PSCs [125]. Taking nano prisms NaYF4: Yb^{3+}, Er^{3+}, which is hydrothermally formed to the TiO_2 layer in PSCs, the efficiency enhancement has been demonstrated by Roh *et al.* [126]. In another study, Wang *et al.* introduced efficiency increment via hydrothermally grown 3% Er^{3+} and 6% Yb^{3+} co-doped TiO_2 nanorod in PSCs [127]. In 2016, He *et al.* integrated $NaYF_4$:Yb^{3+}, Er^{3+} nanoparticles as mesoporous electrode with PSCs ($CH_3NH3PbI_3$ based), this leads a short circuit current density 0.74 mAcm^{-2} excite with 980 nm laser with

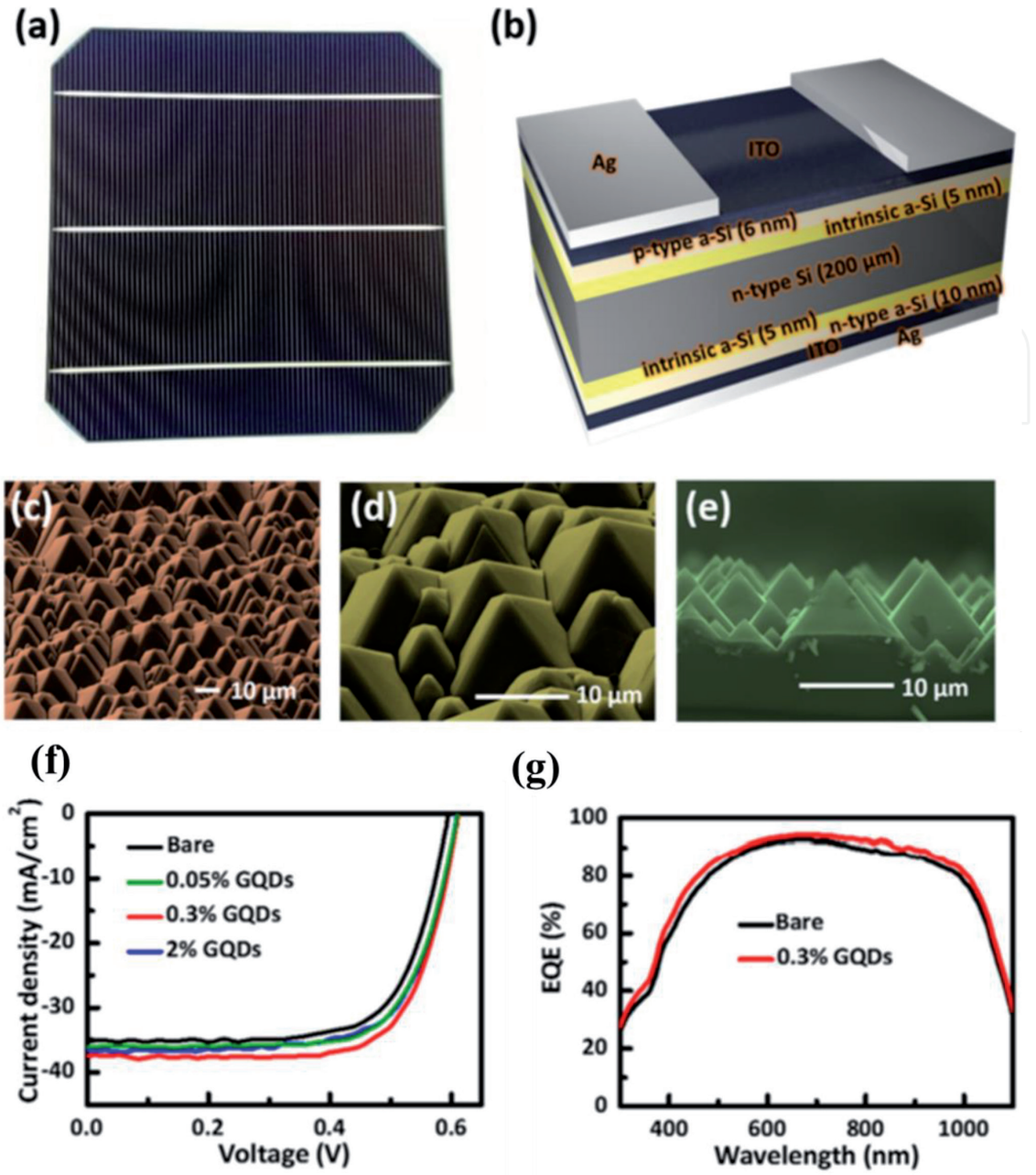

Figure 8.
(a) Photographic image, (b) schematic, (c) low-resolution, (d) high-resolution, and (e) cross-sectional SEM images of SHJ solar cells. (f) J – V characteristics of SHJ solar cells with various concentrations of GQDs. (g) EQE spectra of SHJ solar cells without and with 0.3 wt % of GQDs. Reprinted with permission from [116]. Copyright (2016) American Chemical Society.

28 W cm^{-2} [128]. The sample (semiconductor plasmon-sensitized nanocomposites i.e. $mCu_{2-x}S@SiO_2@ Er_2O_3$), which changes the broadband infrared light to visible light by the localized surface plasmon resonance (LSPR) of $Cu_{2-x}S$ integrated with TiO_2 paste [129]. This arrangement is used in PSCs as an electron extraction layer with an enhanced response of 800–1000 nm. With the dependency of the power density of the 980 nm extraction layer (>0.85 $mAcm^{-2}$), the short circuit current density was noticed to rise 45 Wcm^{-2}.

6. Recent developments on 2d perovskite photovoltaic cells

The 2d layered perovskites are more advanced and useful than their 3d structures. The unique electroluminescent property of 2d perovskites makes them more

superior to their 3d counterparts. 2d perovskites structures have large exciton binding energy than 3d structures [130–131]. Due to this fact, 2d perovskite has a high photoluminescence quantum yield (PLQY) with enhanced radiative recombination. The appearance of cascaded energy structures in 2d perovskites films (mixed n layer thickness) leads to a fast and efficient energy transfer from lower-n quantum wells to higher-n quantum wells. These results in the decreased exciton quenching effect: occurring the enhanced van der Walls interactions in organic molecules and hydrophobic organic ligands, 2d perovskites show enhanced and ambient and thermal stability in the comparison with 3d perovskites. In 2d perovskites, the electrical and optical properties can be tuned more and advanced applications like circular-polarized emission and broadband emission due to their excellent chemical tenability [132–135].

You *et al.* [136] developed a novel annealing approach formethylammonium lead iodide ($MAPbI_3$) and $(CsPbI_3)_{0.05}(FAPbI_3)_{0.95}(MAPbBr_3)_{0.05}$ mixed perovskite

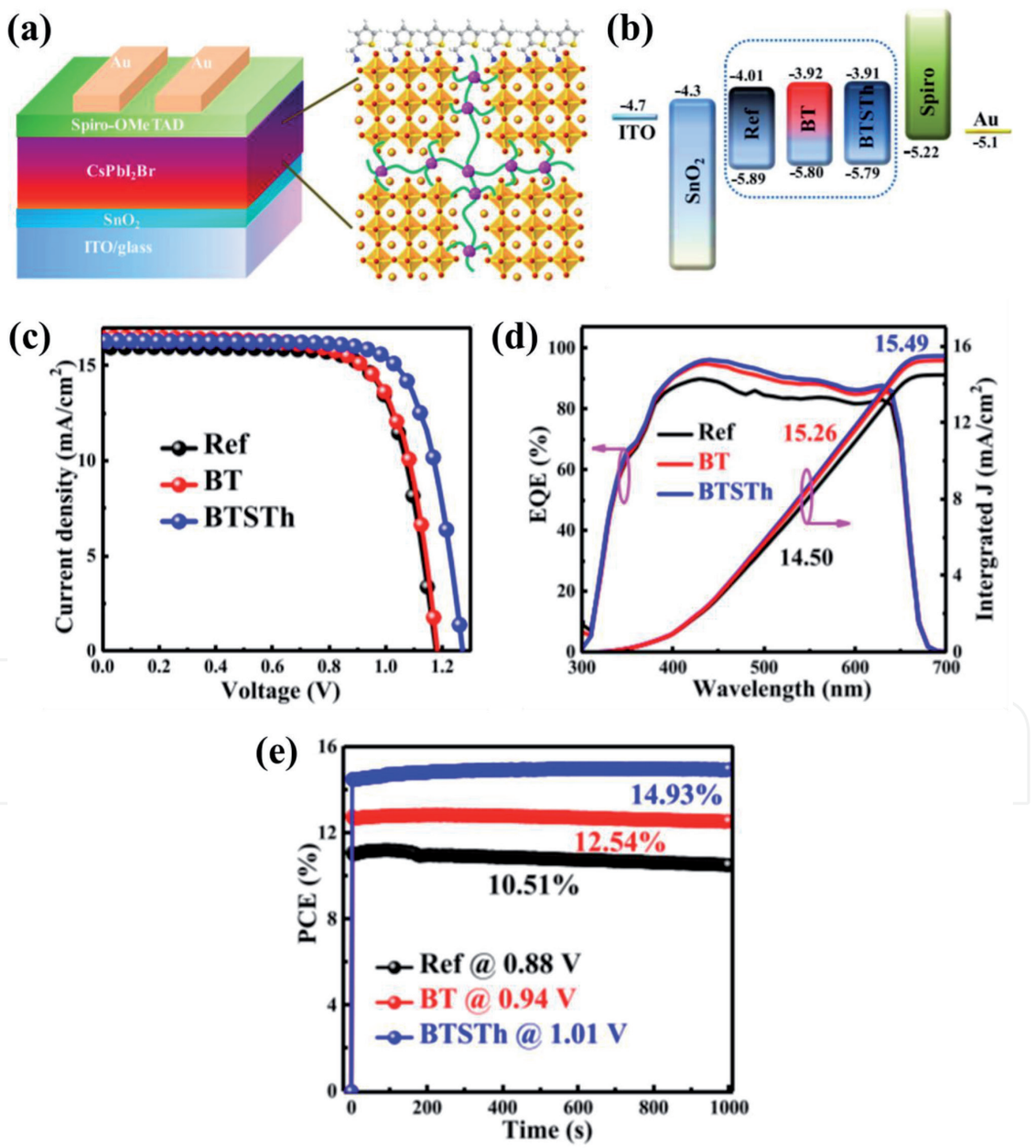

Figure 9.
(a) Schematic illustration of the device and the dual-protection $CsPbI_2Br$ film. (b) Band alignment between various layers of a complete device. (c) the J – V curves of the devices fabricated from the ref., BT, and BTSTh films. (d) the EQE spectra of the various devices. (e) the stabilized maximum power output of the devices. Reprinted with permission from [140]. Copyright (2020) American Chemical Society.

films by fast laser beam scanning. Under optimum conditions, high-quality perovskite films with good crystallinity, preferred orientation, and low density of defects device offers PCE nearly about 20%. Wang *et al.* [137] showed an efficient strategy to tune the band structure and electron mobility of the ETL by adding NH_4Cl to the sol–gel-derived ZnO precursor. Low temperature (160°C) fabricated $CsPbIBr_2$solar cells recorded high efficiency of 10.16%. Li *et al.* [138] fabricated the $MAPbI_3$perovskite solar cells and showed the device performance is strongly influenced by the TiO_2 electron transport layer. Oz *et al.* [139] studied the effect of lead(II)propionate additive on the stabilization of $CsPbI_2Br$all-inorganic perovskite, and the use of a novel dopant-freepolymer hole transport material (synthesized by us) for photovoltaic performance assessment of $CsPbI_2Br$ solar cells.

Fu and his co-workers report a dual-protection strategy via incorporating monomer trimethylolpropane triacrylate (TMTA) into$CsPbI_2Br$ perovskite bulk and capping the surface with 2-thiophenemethylammonium iodide (Th – NI) [140]. The fabricated devices show a greatly improved efficiency from 12.17 to 15.58% with an opening circuit voltage (V_{oc}) of 1.286 V. **Figure 9a** presents a schematic illustration of the device and the dual-protection $CsPbI_2Br$ film. The UPS measurements are conducted to reveal the electronic structure changes the calculated results are drawn in **Figure 9b**. The photocurrent density-voltage (J-V) curves of the optimal devices under AM 1.5 illumination are presented in **Figure 9c.** The ref. device shows the best efficiency of 12.17% with a V_{oc} of 1.151 V, and TMTA doped film (BT) devices show an improved efficiency of 13.88% after incorporating 1 mg/mL of TMTA. In **Figure 9e**, the Th – NI modified BT film (BTSTh) device exhibits the improved output efficiency with 14.93% for 1000 s, while the ref. shows the attenuated efficiency and remains 10.51% under the same operation, which indicates the better operational stability for the BTSTh devices.

Li *et al.* [141] reported vertically aligned 2D/3D Pb – Sn perovskites with enhanced charge extraction and suppressed phase segregation for efficient printable solar cells. Wang *et al.* [142] successfully fabricated high-quality $CsPbBr_3$ films via additive engineering with NH_4SCN. The incorporation of NH_4^+ and pseudo-halide ion SCN^- into the precursor solution, a smooth and dense $CsPbBr_3$ film with good crystallinity and low trap state density can be obtained.

7. Neoteric challenges in development of 2d photovoltaic cells

It is crucial that the entire energy of any absorbed photon is harvested for next-generation photovoltaics. The unique features of 2d layered materials such as high crystalline quality, transparency, atomic thickness, make them special to use in photovoltaic solar cells. Thus, it is important to synthesized and demonstrate 2d flexible photovoltaic devices on industrial scale. While some different issues and problems will be faced by the experimentalist regarding an efficiency performance. The specific requirements in the fabrication of photovoltaic devices are the large-area synthesis, highly controllable, low cost, atomically thin, and recyclable fabrication of materials and their devices. The above features are specified not only for all potential electronic devices but also for optoelectronic devices. Increased number of layers of 2d materials, the conductivity of the material improves at the cost of reduced transparency. The application of 2dmaterials like TMDs and perovskites in photovoltaic devices has also been investigated over the last few years. The advantages of using such materials for solar cells have been explored based on the high absorption coefficient of these materials in the visible to the near-infrared part of the solar spectrum. So there is a need for more investigation of the hetero-structure based on these materials, which can synergize the performance of the

device. Although the efficiency of perovskite solar cells has been boosted to over 25%, further improving the efficiency towards their theoretical Shockley–Queisser efficiency limit of more than 30% and improving the stability towards commercial application deserve more intensive research. The micromechanical cleavage method provides us structural study and device performance but this cannot be used as industry level as low production rate and low yield. This lack noted by the scientific community and remarkable advancement has been achieved by fabricating 2d materials at the industry level within the past few years. Moreover, TMDs, hBN, graphene, and perovskite are critically fabricated with different methods like physical vapor transport, CVD, layer by layer conversion; etc. The samples obtained in this way have properties like controllable thickness, electronic properties scalable sizes, and high crystal quality. Also, a liquid-based wet chemical method provides two unique requirements high control power and low-cost manufacturing of atomically thin 2D nanomaterials. Moreover, it is necessary to achieve excellent crystal quality and film uniformity before using the LBWC technique in large scale manufacturing.

8. Conclusion

In this chapter, we have enlightened specific properties and synthesis techniques of graphene, TMDs, and perovskite. We have described recent progress made with graphene, graphene-based 2D materials for solar photovoltaics. In addition, 2d Schottky junction, homojunction, and heterojunction are explained briefly. The unique account of the charge carrier transport layer as ETL and HTL has been done fairly. Moreover, regular n-i-p and inverted p-i-n structure are the key features. Furthermore, 2DRP perovskite, upconversion/downconversion of perovskite cells are also discussed briefly. In the last of the section very recent developments on 2d perovskite photovoltaic cells have been critically explained with the facts. Various challenges in the fabrication and development of today's devices are pointed out. Therefore, the outlook towards 2d materials should be optimistic and needs more attention in the near future.

Author details

Manoj Kumar Singh[1*], Pratik V. Shinde[2], Pratap Singh[1] and Pawan Kumar Tyagi[3]

1 Department of Physics under School of Engineering and Technology (SOET), Central University of Haryana (CUH), Mahendergarh, Haryana, India

2 Centre for Nano and Material Sciences, Jain University, Bangalore, India

3 Department of Applied Physics, Delhi Technological University, Delhi, India

*Address all correspondence to: manojksingh@cuh.ac.in

References

[1] Bequerel ER. C.R.Acad.Sci. 1839;9 145-149.

[2] Park NG. Research Direction toward Scalable, Stable, and High Efficiency Perovskite Solar Cells. Advanced Energy Materials 2020;10 1903106(1-14). DIO: 10.1002/aenm.201903106.

[3] Solanki CS and Beaucarne G. Advanced solar cell concepts. Energy for Sustainable Development 2007;11 17-23. DOI: 10.1016/S0973-0826(08)60573-6.

[4] Wang L, Huang L, Wee Tan WC, Feng X, Chen L, Huang X, et al. 2D Photovoltaic Devices: Progress and Prospects. Small method 2018;2 1700294 (1-20). DOI: 10.1002/smtd.201700294

[5] Edvinsson T. Optical quantum confinement and photocatalytic properties in two-, one- and zero-dimensional nanostructures. Royal Society Open Science 2018;5 180387-180403. DOI: 10.1098/rsos.180387.

[6] Butler SZ, Hollen SM, Cao L, Cui Y, Gupta JA, Gutierrez HR, et al. Progress, Challenges, and Opportunities in Two-Dimensional Materials Beyond Graphene. ACS Nano 2013;7 2898-2926. DOI: 10.1021/nn400280c.

[7] Gupta A, Sakthivel T, Seal S. Recent development in 2D materials beyond graphene. Progress in Materials Science 2015;73 44-126. DOI: 10.1016/j.pmatsci.2015.02.002.

[8] Chen L, Zhang C, Liu. The Optimal Electronic Structure for High-Mobility 2D Semiconductors: Exceptionally High Hole Mobility in 2D Antimony. Journal of American Chemical Society 2019;141 16296-16302. DOI: 10.1021/jacs.9b05923.

[9] Song H, Liu J, Liu B, Wu J, Cheng HM, Kang F. Two-Dimensional Materials for Thermal Management Applications. Joule 2018;2 442-463. DOI: 10.1016/j.joule.2018.01.006.

[10] Zhang H, Ultrathin Two-Dimensional Nanomaterials, ACS Nano 2015;9 9451-9469. DOI: 10.1021/acsnano.5b05040.

[11] Guo Y. Surface chemical-modification for engineering the intrinsic physical properties of inorganic two-dimensional nanomaterials. Chemical Society Review 2015;44 637-646. DOI: 10.1039/C4CS00302K.

[12] Zhang Y, Tan YW, Stormer HL, Kim P. Experimental observation of the quantum Hall effect and Berry's phase in graphene. Nature Letters 2005;438 201-204. DOI: 10.1038/nature04235.

[13] Novoselov KS, Jiang Z, Zhang Y, Morozov SV, Stormer HL, Zeitler U et al. Room-Temperature Quantum Hall Effect in Graphene. Science 2007;315 1379. DOI: 10.1126/science.1137201.

[14] Stoller MD, Park S, Zhu Y, An J, Ruoff RS. Graphene-Based Ultracapacitors 2008;8 3498-3502. DOI: 10.1021/nl802558y.

[15] Pomerantseva E, Gogotsi Y. Two-dimensional heterostructures for energy storage. Nature Energy 2017;2(7) 1-6. DOI: 10.1038/nenergy.2017.89.

[16] Tucek J, Btonski P, Ugolotti P, Swain AK, Enokib T, Zboril R. Emerging chemical strategies for imprinting magnetism in graphene and related 2D materials for spintronic and biomedical applications. Chemical Society Reviews 2018;47 3899-3990. DOI: 10.1039/C7CS00288B.

[17] Georgakilas V, Perman JA, Tucek J, Zboril R. Broad family of carbon nanoallotropes: classification, chemistry, and applications of

fullerenes, carbon dots, nanotubes, graphene, nanodiamonds, and combined superstructures. Chemical Reviews 2015;115 4744-4822. DOI: 10.1021/cr500304f.

[18] Novoselov KS, Geim AK, Morozov SV, Jiang D, Zhang D, Dubonos SV et al. Electric Field Effect in Atomically Thin Carbon Films. Science 2004;306(5696) 666-669. DOI: 10.1126/science.1102896.

[19] Allen MJ, Tung VC, Kaner RB. Honeycomb Carbon: A Review of Graphene. Chemical Reviews 2010;110 132-145. DOI: 10.1021/cr900070d.

[20] Mahmoodi T, Wang Y, Hahn YB. Graphene and its derivatives for solar cells application. Nano Energy 2018;47 51-65. DOI: 10.1016/j.nanoen.2018.02.047.

[21] Akinwande D, Brennan CJ, Bunch JS, Egberts P, Felts JR, Gao H et al. A review on mechanics and mechanical properties of 2D materials-Graphene and beyond. Extreme Mechanics Letters 2017;13 42-77. DOI: 10.1016/j.eml.2017.01.008.

[22] Yu1 X, Cheng H, Zhang M, Zhao Y, Qu L. Graphene-based smart materials, Nature Reviews Materials 2017;2 1-13. DOI: 10.1038/natrevmats.2017.46.

[23] Das S, Pandey D, Thomas J, Roy. The Role of Graphene and Other 2D Materials in Solar Photovoltaics. Advanced Materials 2018;31(1) 1802722(1-35). DOI: 10.1002/adma.201802722.

[24] Cao M, Xiong DB, Yang L, Li S, Xie Y, Guo Q et al. Ultrahigh Electrical Conductivity of Graphene Embedded in Metals, Advanced Functional Materials 2019;29(17) 1806792(1-8). DOI: 10.1002/adfm.201806792.

[25] Ma Y, Zhi L. Graphene-Based Transparent Conductive Films: Material Systems, Preparation and Applications. Small Methods 2018;3(1) 1800199(1-32). DOI: 10.1002/smtd.201800199.

[26] Liu N, Chortos A, Lei T, Jin L, KimTR, Bae WG et al., Ultratransparent and stretchable graphene electrodes, Science Advances 2017;3 1700159(1-10). DOI: 10.1126/sciadv.1700159.

[27] Adetayo A, Runsewe D. Synthesis and Fabrication of Graphene and Graphene Oxide: A Review. Open Journal of Composite Materials 2019;9 207-229. DOI: 10.4236/ojcm.2019.92012.

[28] Das S, Sudhagar P, Kang YS, Choi W. Synthesis and Characterization of Graphene. In: Lu W Baek JB, Dai L (ed.) Carbon Nanomaterials for Advanced Energy Systems: Advances in Materials Synthesis and Device Applications. John Wiley & Sons; 2015. p1-2.

[29] Somani PR, Somani SP, Umeno M. Planer nano-graphenes from camphor by CVD. Chemical Physics Letters 2006;430 56-59. DOI: 10.1016/j.cplett.2006.06.081.

[30] Obraztsov AN, Obraztsova EA, Tyurnina AV, Zolotukhin AA. Chemical vapor deposition of thin graphite films of nanometer thickness. Carbon 2007;45 2017-2021. DOI: 10.1016/j.carbon.2007.05.028.

[31] Li X, Cai1 W, An1 J, Kim, Nah J, Yang D et al. Large-Area Synthesis of High-Quality and Uniform Graphene Films on Copper Foils. Science 2009;324 1312-1314. DOI: 10.1126/science.1171245.

[32] Cheng R, Jiang S, Chen Y, Liu Y, Weiss, Cheng HC et al. Few-layer molybdenum disulfide transistors and circuits for high-speed flexible electronics. Nature Communications 2014;5 5143(1-9). DOI: 10.1038/ncomms6143.

[33] Akinwande D, Petrone N, Hone J. Two-dimensional flexible

nanoelectronics. Nature Communications 2014;5 5678(1-12). DOI: 10.1038/ncomms6678.

[34] Choi W, Choudhary N, Han GH, Park J, Akinwande D, Lee YH. Recent development of two-dimensional transition metal dichalcogenides and their applications. Materialstoday 2017;20(3) 116-130. DOI: 10.1016/j.mattod.2016.10.002.

[35] Li C, Cao Q, Wang F, Xiao Y, Li Y, Delaunay JJ et al. Engineering graphene and TMDs based van der Waals heterostructures for photovoltaic and photoelectrochemical solar energy conversion. Chemical Society Reviews 2018;47 4981-5037. DOI: 10.1039/C8CS00067K.

[36] Wang QH, Zadeh KK, Kis A, Coleman JN, Strano MS. Electronics and optoelectronics of two-dimensional transition metal dichalcogenides. Nature nanotechnology 2012;7 699-712. DOI: 10.1038/nnano.2012.193

[37] Mak KF, Lee C, Hone J, Shan J, Heinz TF. Atomically thin MoS2: a new direct-gap semiconductor. Physical Review Letters 2010;105 136805(1-4). DOI: 10.1103/PhysRevLett.105.136805.

[38] Mak KF, He K, Lee C, Lee GH, Hone J, Heinz TF et al. Tightly bound trions in monolayer MoS_2. Nature Materials 2013;12 207-211. DOI: 10.1038/nmat3505.

[39] Cao T, Wang G, Han W, Ye H, Zhu C, Shi J et al. Valley-selective circular dichroism of monolayer molybdenum disulphide. Nature Communications 2012;3 1-5. DOI: 10.1038/ncomms1882.

[40] Wilson JA, Yoffe AD. The transition metal dichalcogenides discussion and interpretation of the observed optical, electrical and structural properties. Advances in Physics 1969;18(73) 193-335. DOI: 10.1080/00018736900101307.

[41] Velicky M, Toth PS. From two-dimensional materials to their heterostructures: An electrochemist's perspective. Applied Materials Today 2017;8 68-103. DOI: 10.1016/j.apmt.2017.05.003.

[42] Simone Bertolazzi, Jacopo Brivio, Kis A. Stretching and Breaking of Ultrathin MoS_2. ACS Nano 2011; 5 9703-9709. DOI: 10.1021/nn203879f.

[43] Iqbal MZ, Alam S, Faisal MM, Khan S. Recent advancement in the performance of solar cells by incorporating transition metal dichalcogenides as counter electrode and photoabsorber. International Journal of Energy Research 2019; 43 3058-3079. DOI: 10.1002/er.4375.

[44] Ansari SA, Fouad H, Ansari SG, Sk MP, Cho MH. Mechanically exfoliated MoS_2 sheet coupled with conductive polyaniline as a superior supercapacitor electrode material. Journal of colloid and interface science 2017;504 276-282. DOI: 10.1016/j.jcis.2017.05.064.

[45] Ding W, Hu L, Dai J, Tang X, Wei R, Sheng Z, et al. Highly ambient-stable 1T-MoS_2 and 1T-WS_2 by hydrothermal synthesis under high magnetic fields. ACS nano 2019;13(2) 1694-1702. DOI: 10.1021/acsnano.8b07744.

[46] Chae WH, Cain JD, Hanson ED, Murthy AA, Dravid VP. Substrate-induced strain and charge doping in CVD-grown monolayer MoS_2. Applied Physics Letters 2017;111(14) 143106(1-5). DOI: 10.1063/1.4998284.

[47] Zhan L, Wan W, Zhu Z, Shih TM, Cai W. MoS_2 materials synthesized on SiO_2/Si substrates via MBE. Journal of Physics: Conference Series 2017;864(1) 012037(1-4). DOI: 10.1088/1742-6596/864/1/012037.

[48] Yang J, Liu L. Trickle Flow Aided Atomic Layer Deposition (ALD)

Strategy for Ultrathin Molybdenum Disulfide (MoS_2) Synthesis. ACS applied materials & interfaces 2019;11(39) 36270. DOI: 10.1021/acsami.9b12023.

[49] Xiao M, Huang F, W Huang, Dkhissi Y, Zhu Y, Etheridge J, et al. A Fast Deposition Crystallization Procedure for Highly Efficient Lead Iodide Perovskite Thin Film Solar Cells. Angewandte Chemie 2014; 126(37)10056-10061. DOI: 10.1002/ange.201405334.

[50] Cai B, Xing Y, Yang Z, Zhang WH, Qiu J, High performance hybrid solar cells sensitized by organolead halide perovskites. Energy Environmental Science 2013;**6** 1480-1485. DOI: 10.1039/C3EE40343B.

[51] Lan C, Zhou Z, Wei R, Ho JC, Two-dimensional perovskite materials: From synthesis to energy-related applications. Materials Today Energy 2019;11 61-82. DOI: 10.1016/j.mtener.2018.10.008.

[52] Kulkarni SA, Mhaisalkar SG, Mathews N, Boix PP. Perovskite Nanoparticles: Synthesis, Properties, and Novel Applications in Photovoltaics and LEDs. Small Methods 2019;3 1800231(1-16). DOI: 10.1002/smtd.201800231.

[53] Ha ST, Liu X, Zhang Q, Giovanni D, Sum TC, Xiong Q. Synthesis of Organic–Inorganic Lead Halide Perovskite Nanoplatelets: Towards High-Performance Perovskite Solar Cells and Optoelectronic Devices. Advanced Optical Materials 2014;2 838-844. DOI: 10.1002/adom.201400106.

[54] Utama MIB, Mata M, Magen C, Arbiol J, Xiong Q. Twinning-, Polytypism-, and Polarity-Induced Morphological Modulation in Nonplanar Nanostructures with van de Waals Epitaxy. Advanced Functional Materials 2013;23 1636-1646. DOI: 10.1002/adfm.201202027.

[55] Utama MIB, Peng ZP, Chen R, Peng B, Xu XL, Dong YJ, et al. Vertically Aligned Cadmium Chalcogenide Nanowire Arrays on Muscovite Mica: A Demonstration of Epitaxial Growth Strategy. Nano Letters 2011;11 3051-3057. DOI: 10.1021/nl1034495.

[56] Gillet M, Delamare R, Gillet E. Growth of epitaxial tungsten oxide nanorods. Journal of Crystal Growth 2005;279 93-99. DOI: 10.1016/j.jcrysgro.2005.01.089.

[57] Tan C, Cao X, Wu XJ, He Q, Yang J, Zhang, et al. Recent advances in ultrathin two-dimensional nanomaterials. Chemical Reviews 2017;117(9) 6225-6331. DOI: 10.1021/acs.chemrev.6b00558.

[58] Fontana M, Deppe T, Boyd AK, Rinzan M, Liu AY, Paranjape M. Electron-hole transport and photovoltaic effect in gated MoS_2 Schottky junctions. Scientific Reports 2013;3 1634(1-5). DOI: 10.1038/srep01634.

[59] Shin DH, Kim JH, Kim JH, Jang CW, Seo SW, Lee HS, Kim S, Choi SH. Graphene/porous silicon Schottky-junction solar cells. Journal of Alloys and Compounds 2017;715:291-296. DOI: 10.1016/j.jallcom.2017.05.001.

[60] Yi SG, Kim SH, Park S, Oh D, Choi HY, Lee N, et al. Mo_{1-X} W_X Se_2-Based Schottky Junction Photovoltaic Cells. ACS applied materials & interfaces 2016;8(49) 33811-33820. DOI: 10.1021/acsami.6b11768.

[61] Pospischil A, Furchi M M, Mueller T. Solar-energy conversion and light emission in an atomic monolayer p-n diode. Nature Nanotechnology 2014;9(4), 257-261. DOI: 10.1038/nnano.2014.14

[62] Baugher BW, Churchill HO, Yang Y, Herrero PJ. Optoelectronic devices based on electrically tunable p-n diodes

in a monolayer dichalcogenide. Nature Nanotechnology 2014;9(4) 262(1-6). DOI: 10.1038/nnano.2014.25.

[63] Ross JS, Klement P, Jones AM, Ghimire NJ, Yan J. Electrically tunable excitonic light-emitting diodes based on monolayer WSe2 p-n junctions. Nature Nanotechnology 2014;9(4) 268-272. DOI: 10.1038/nnano.2014.26.

[64] Memaran S, Pradhan NR, Lu Z, Rhodes D, Ludwig J, Zhou Q, et al. Pronounced Photovoltaic Response from Multilayered Transition-Metal Dichalcogenides PN-Junctions. Nano Letters 2015;15(11) 7532-7538. DOI: 10.1021/acs.nanolett.5b03265.

[65] Li L, Yu Y, Ye GJ, Ge Q, Ou X, Wu H et al. Black phosphorus field-effect transistors. Nature Nanotechnology 2014;9(5) 372-377. DOI: 10.1038/nnano.2014.35.

[66] Liu H, Neal AT, Zhu Z, Luo Z, Xu X, Tomanek D et al, Phosphorene: An Unexplored 2D Semiconductor with a High Hole Mobility. ACS Nano 2014;8(4) 4033-4041. DOI: 10.1021/nn501226z.

[67] Xia F, Wang H, Jia Y. Rediscovering black phosphorus as an anisotropic layered material for optoelectronics and electronics. Nature Communications 2014;5 4458(1-6). DOI: 10.1038/ncomms5458.

[68] Choi MS, Qu D, Lee D, Liu X, Watanabe K, Taniguchi T et al. Lateral MoS_2 p–n junction formed by chemical doping for use in high-performance optoelectronics. ACS nano 2014;8(9) 9332-9340. DOI: 10.1021/nn503284n.

[69] Duan X, Wang C, Shaw JC, Cheng R, Chen Y, Li H et al. Lateral epitaxial growth of two-dimensional layered semiconductor heterojunctions. Nature nanotechnology 2014;9(12) 1024-1030. DOI: 10.1038/nnano.2014.222.

[70] Gong Y, Lin J, Wang X, Shi G, Lei S, Lin Z, et al. Vertical and in-plane heterostructures from WS_2/MoS_2 monolayers. Nature materials 2014;13(12) 1135-1142. DOI: 10.1038/nmat4091.

[71] Li Z, Zheng J, Zhang Y, Zheng C, Woon WY, Chuang MC. et al. Synthesis of ultrathin composition graded doped lateral WSe_2/WS_2 heterostructures. ACS Applied Materials & Interfaces 2017;9(39) 34204-34212. DOI: 10.1021/acsami.7b08668.

[72] Snaith HJ, Abate A, Ball JM, Eperon GE, Leijtens T, Noel NK. et al. Anomalous Hysteresis in Perovskite Solar Cells. The Journal of Physical Chemistry Letters 2014;5 1511-1515. DOI: 10.1021/jz500113x.

[73] Baena JPC, Steier L, Tress W, Saliba M, Neutzner S, Matsui T, Highly efficient planar perovskite solar cells through band alignment engineering. Energy Environmental Science 2015;5 2928-2934. DOI: 10.1039/C5EE02608C.

[74] Guo Z, Zhuang J, Ma Z, Xia H, Yi J, Zhou W, et al. Improving the performance of lead acetate-based perovskite solar cells via solvent vapor annealing, Adv. Funct. Mater. 2019;21 4753-4762. DOI: 10.1039/C9CE00724E.

[75] Roose B, Wang Q, Abate A. The Role of Charge Selective Contacts in Perovskite Solar Cell Stability, Advanced Energy Materials 9 (2018) 1803140-1803159. DOI: 10.1002/aenm.201803140.

[76] Posudievsky OY, Konoshchuk NV, Shkavro AG, Koshechko VG, Pokhodenko VD. Structure and electronic properties of poly(3,4-ethylenedioxythiophene) poly(styrene sulfonate) prepared under ultrasonic irradiation. Synthetic Metals 2014;195 335-339. DOI: 10.1016/j.synthmet.2014.07.001.

[77] Singh R, Giri A, Pal M, Thiyagarajan K, Kwak J, Lee JJ, Perovskite solar cells with an MoS_2 electron transport layer. Journal of Materials Chemistry A 2019;7 7151-7158. DOI: 10.1039/C8TA12254G.

[78] Yin G, Zhao H, Feng J, Sun J, Yan J, Liu Z, et al. Low-temperature and facile solution-processed two-dimensional TiS 2 as an effective electron transport layer for UV-stable planar perovskite solar cells. Journal of Materials Chemistry A. 2018;6(19):9132-9138. DOI: 10.1039/C8TA01143E.

[79] Huang P, Chen Q, Zhang K, Yuan L, Zhou Y, Song B, et al. 21.7% efficiency achieved in planar n–i–p perovskite solar cells via interface engineering with water-soluble 2D TiS_2. Journal of Materials Chemistry A 2019;7(11) 6213-6219. DOI: 10.1039/C8TA11841H.

[80] Zhao X, Liu S, Zhang H, Chang SY, Huang W, Zhu B, et al. 20% efficient perovskite solar cells with 2D electron transporting layer. Advanced Functional Materials 2019;29(4) 1805168(1-8). DIO: 10.1002/adfm.201805168.

[81] Yang L, Dall'Agnese Y, Hantanasirisakul K, Shuck CE, Maleski K, Alhabeb M, SnO_2–Ti_3C_2 MXene electron transport layers for perovskite solar cells. Journal of materials chemistry A 2019;7(10) 5635-5642. DOI: 10.1039/C8TA12140K.

[82] Guo Z, Gao L, Xu Z, Teo S, Zhang C, Kamata Y et al. High Electrical Conductivity 2D MXene Serves as Additive of Perovskite for Efficient Solar Cells. Small 2018;14 1802738(1-8). DOI: 10.1002/smll.201802738.

[83] Wang Y, Zhang H, Zhang T, Shi W, Kan M, Chen J et al. Photostability of $MAPbI_3$ perovskite solar cells by incorporating black phosphorus. Solar RRL 2019;3(9) 1900197(1-7). DOI: 10.1002/solr.201900197.

[84] Long R, Fang W, Akimov AV. Nonradiative electron–hole recombination rate is greatly reduced by defects in monolayer black phosphorus: ab initio time domain study. The Journal of Physical Chemistry Letters 2016;7(4) 653-659. DOI: 10.1021/acs.jpclett.6b00001.

[85] Capasso A, Matteocci F, Najafi L, Prato M, Buha J, Cinà L et al. Few Layer MoS_2 Flakes as Active Buffer Layer for Stable Perovskite Solar Cells. Advanced Energy Materials 2016;6(16) 1600920(1-12). DOI: 10.1002/aenm.201600920.

[86] Jawaid A, Nepal D, Park K, Jespersen M, Qualley A, Mirau P, et al. Mechanism for liquid phase exfoliation of MoS_2. Chemistry of Materials 2016;28(1) 337-348. DOI: 10.1021/acs.chemmater.5b04224.

[87] Gupta A, Arunachalam V, Vasudevan S. Liquid-phase exfoliation of MoS_2 nanosheets: the critical role of trace water. The journal of physical chemistry letters 2016;7(23) 4884-4890. DOI: 10.1021/acs.jpclett.6b02405.

[88] Najafi L, Taheri B, Martín-García B, Bellani S, Girolamo DD, Agresti A, et al. MoS_2 quantum dot/graphene hybrids for advanced interface engineering of a $CH_3NH_3PbI_3$ perovskite solar cell with an efficiency of over 20%. ACS nano 2018;12(11) 10736-10754. DOI: 10.1021/acsnano.8b05514.

[89] Meng L, You J, Guo TF, Yang Y. Recent advances in the inverted planar structure of perovskite solar cells. Accounts of chemical research 2016;49(1) 155-165. DOI: 10.1021/acs.accounts.5b00404.

[90] Huang L, Xu J, Sun X, Du Y, Cai H, Ni J, et al. Toward revealing the critical role of perovskite coverage in highly efficient electron-transport layer-free perovskite solar cells: an energy band and equivalent circuit model

perspective. ACS Applied Materials & Interfaces 2016;8(15) 9811-9820. DOI: 10.1021/acsami.6b00544.

[91] Jeng JY, Chiang YF, Lee MH, Peng SR, Guo TF, Chen P, et al. $CH_3NH_3PbI_3$ perovskite/fullerene planar heterojunction hybrid solar cells. Advanced Materials 2013;25(27) 3727-3732. DOI: 10.1002/adma.201301327.

[92] Hu Q, Wu J, Jiang C, Liu T, Que X, Zhu R, et al. Engineering of electron-selective contact for perovskite solar cells with efficiency exceeding 15%. ACS nano. 2014;8(10) 10161-10167. DOI: doi.org/10.1021/nn5029828.

[93] Liu D, Yang J, Kelly TL. Compact layer free perovskite solar cells with 13.5% efficiency. Journal of the American Chemical Society 2014;136(49) 17116-17122. DOI: 10.1021/ja508758k.

[94] Ke W, Fang G, Wan J, Tao H, Liu Q, Xiong L, et al. Efficient hole-blocking layer-free planar halide perovskite thin-film solar cells. Nature communications 2015;6(1) 1-7. DOI: 10.1038/ncomms7700.

[95] Chen Z, Dong Q, Liu Y, Bao C, Fang Y, Lin Y, et al. Thin single crystal perovskite solar cells to harvest below-bandgap light absorption. Nature communications. 2017;8(1) 1-7. DOI: 10.1038/s41467-017-02039-5.

[96] Prochowicz D, Yadav P, Saliba M, Saski M, Zakeeruddin SM, Lewiński J, et al. Mechanosynthesis of pure phase mixed-cation $MA_XFA_{1-X}PbI_3$ hybrid perovskites: photovoltaic performance and electrochemical properties. Sustainable Energy & Fuels 2017;1(4) 689-693. DOI: 10.1039/C7SE00094D.

[97] Yang W, Chen J, Lian X, Li J, Yao F, Wu G, et al. Black Phosphorus Quantum Dots Induced High Quality Perovskite Film for Efficient and Thermally Stable Planar Perovskite Solar Cells. Solar Rrl. 2019;3(8) 1900132(1-8). DOI: 10.1002/solr.201900132.

[98] Giorgi G, Yamashita K, Palummo M. Nature of the electronic and optical excitations of Ruddlesden–Popper hybrid organic–inorganic perovskites: The role of the many-body interactions. The journal of physical chemistry letters 2018;9(19) 5891-5896. DOI: 10.1021/acs.jpclett.8b02653.

[99] Zheng Y, Niu T, Ran X, Qiu J, Li B, Xia Y, et al. Unique characteristics of 2D Ruddlesden–Popper (2DRP) perovskite for future photovoltaic application. Journal of Materials Chemistry A.2019;7(23):13860-13872. DOI: 10.1039/C9TA03217G.

[100] Gao X, Zhang X, Yin W, Wang H, Hu Y, Zhang Q, et al. Ruddlesden–Popper Perovskites: Synthesis and Optical Properties for Optoelectronic Applications. Advanced Science 2019;6(22) 1900941(1-22). DOI: 10.1002/advs.201900941.

[101] Smith IC, Hoke ET, Solis-Ibarra D, McGehee MD, Karunadasa HI. A Layered Hybrid Perovskite Solar-Cell Absorber with Enhanced Moisture Stability. Angewandte International Edition Chemie 2014;53 11232-11235. DOI: 10.1002/anie.201406466.

[102] Mitzi DB, Templating and structural engineering in organic–inorganic perovskites. J. Chem. Soc., Dalton Transaction 2001 1-12. DOI: 10.1039/B007070J.

[103] Quan LN, Yuan M, Comin R, Voznyy O, Beauregard EM, Hoogland S et al. Ligand-Stabilized Reduced-Dimensionality Perovskites Journal of American Chemical Society 2016;138 2649-2655. DOI: 10.1021/jacs.5b11740.

[104] Eperon GE, Paterno GM, Sutton RJ, Zampetti A, Haghighirad AA, Cacialli F et al. Inorganic caesium lead

iodide perovskite solar cells. Journal of Materials Chemistry A 2015;3 19688-19695. DOI: 10.1039/C5TA06398A.

[105] Protesescu L, Yakunin S, Bodnarchuk MI, Krieg F, Caputo R, Hendon CH et al. Nanocrystals of Cesium Lead Halide Perovskites ($CsPbX_3$, X = Cl, Br, and I): Novel Optoelectronic Materials Showing Bright Emission with Wide Color Gamut. Nano Letters 2015;5 3692-3696. DOI: 10.1021/nl5048779.

[106] Zhang T, Dar MI, Li G, Xu F, Guo, Gratzel M et al. Bication lead iodide 2D perovskite component to stabilize inorganic a-$CsPbI_3$ perovskite phase for high-efficiency solar cells. Science Advances 2017;3 1700841(1-6). DOI: 10.1126/sciadv.1700841.

[107] Tian X, Zhang Y, Zheng R, Wei D, Liu J. Two-dimensional organic–inorganic hybrid Ruddlesden–Popper perovskite materials: preparation, enhanced stability, and applications in photodetection. Sustainable Energy & Fuels 2020;4(5):2087-2113. DOI: 10.1039/C9SE01181A.

[108] Niu W, Eiden A, Prakash VG, Baumberg JJ. Exfoliation of self-assembled 2D organic-inorganic perovskite semiconductors. Applied Physics Letters 2014;104(17) 171111(1-4). DOI: 10.1063/1.4874846.

[109] Bünzli JCG, Chauvin AS: Lanthanides in solar energy conversion. In Jean-Claude GB, Vitalij KP, (ed.) Handbook on the physics and chemistry of rare earths. Elsevier;2014. p169-281.

[110] Huang X, Han S, Huang W, Liu X. Enhancing solar cell efficiency: the search for luminescent materials as spectral converters. Chemical Society Reviews. 2013;42(1) 173-201. DOI: 10.1039/c2cs35288e.

[111] Zhang QY, Yang GF, Jiang ZH. Cooperative downconversion in Gd$Al_3(BO_3)_4$: RE^{3+}, Yb^{3+} (RE= Pr, Tb, and Tm). Applied Physics Letters 2007;91(5) 051903(1-3). DOI: 10.1063/1.2757595.

[112] Li Z, Zeng Y, Qian H, Long R, Xiong Y. Facile synthesis of $GdBO_3$ spindle assemblies and and microdisks as versatile host matrices for lanthanide doping. CrystEngComm. 2012;14(11):3959-3964. DOI: 10.1039/C2CE06596G.

[113] Yuan JL, Zeng XY, Zhao JT, Zhang ZJ, Chen HH, Yang XX. Energy transfer mechanisms in Tb^{3+}, Yb^{3+} codoped Y_2O_3 downconversion phosphor. Journal of Physics D. Applied Physics 2008;41(10) 105406(1-6). DOI: 10.1088/0022-3727/41/10/105406.

[114] Ye S, Zhu B, Chen J, Luo J, Qiu JR. Infrared quantum cutting in Tb^{3+}, Yb^{3+} codoped transparent glass ceramics containing Ca F_2 nanocrystals. Applied Physics Letters 2008;92(14) 141112(1-3). DOI: 10.1063/1.2907496.

[115] Liu X, Ye S, Qiao Y, Dong G, Zhu B, Chen D et al. Cooperative downconversion and near-infrared luminescence of Tb^{3+}–Yb^{3+} codoped lanthanum borogermanate glasses. Applied Physics B 2009;96(1) 51-55. DOI: 10.1007/s00340-009-3478-z.

[116] Tsai ML, Tu WC, Tang L, Wei TC, Wei WR, Lau SP et al. Efficiency enhancement of silicon heterojunction solar cells via photon management using graphene quantum dot as downconverters. Nano letters 2016;16(1) 309-313. DOI: 10.1021/acs.nanolett.5b03814.

[117] Hou X, Xuan T, Sun H, Chen X, Li H, Pan L. High-performance perovskite solar cells by incorporating a $ZnGa_2O_4$: Eu^{3+} nanophosphor in the mesoporous TiO_2 layer. Solar Energy Materials and Solar Cells 2016;149 121-127. DOI: 10.1016/j.solmat.2016.01.021.

[118] Chen W, Luo Q, Zhang C, Shi J, Deng X, Yue L et al. Effects of down-conversion CeO_2: Eu^{3+} nanophosphors in perovskite solar cells. Journal of Materials Science: Materials in Electronics 2017;28(15) 11346-11357. DOI: 10.1007/s10854-017-6928-0.

[119] Wang HQ, Batentschuk M, Osvet A, Pinna L, Brabec CJ. Rare-earth ion doped up-conversion materials for photovoltaic applications. Advanced Materials 2011:2675-2680. DOI: 10.1002/adma.201100511.

[120] Badescu V, Badescu AM. Improved model for solar cells with up-conversion of low-energy photons. Renewable Energy 2009;34(6) 1538-1544. DOI: 10.1016/j.renene.2008.11.006.

[121] Trupke T, Green MA, Würfel P. Improving solar cell efficiencies by up-conversion of sub-band-gap light. Journal of applied physics. 2002;92(7) 4117-4122. DOI: 10.1063/1.1505677.

[122] Pan AC, Canizo CD, Luque A. Characterization of up-converter layers on bifacial silicon solar cells. Materials Science and Engineering: B 2009;159 212-215. DOI: 10.1016/j.mseb.2008.10.058.

[123] Shan GB, Demopoulos GP. Near-infrared sunlight harvesting in dye-sensitized solar cells via the insertion of an upconverter-TiO_2 nanocomposite layer. Advanced materials 2010;22(39) 4373-4377. DOI: 10.1002/adma.201001816.

[124] Shang Y, Hao S, Yang C, Chen G. Enhancing solar cell efficiency using photon upconversion materials. Nanomaterials 2015;5(4) 1782-1809. DOI: 10.3390/nano5041782.

[125] Chen X, Xu W, Song H, Chen C, Xia H, Zhu Y et al. Highly Efficient $LiYF_4$: Yb^{3+}, Er^{3+} Upconversion single crystal under solar cell spectrum excitation and photovoltaic application. ACS Applied Materials & Interfaces 2016;8(14) 9071-9079. DOI: 10.1021/acsami.5b12528.

[126] Roh J, Yu H, Jang J. Hexagonal β-$NaYF_4$: Yb^{3+}, Er^{3+} nanoprism-incorporated upconverting layer in perovskite solar cells for near-infrared sunlight harvesting. ACS Applied Materials & Interfaces 2016;8(31) 19847-19852. DOI: 10.1021/acsami.6b04760.

[127] Wang X, Zhang Z, Qin J, Shi W, Liu Y, Gao H et al. Enhanced photovoltaic performance of perovskite solar cells based on Er-Yb co-doped TiO_2 nanorod arrays. Electrochimica Acta 2017;245 839-845. DOI: 10.1016/J.ELECTACTA.2017.06.032.

[128] He M, Pang X, Liu X, Jiang B, He Y, Snaith H, Lin Z. Monodisperse Dual-functional upconversion nanoparticles enabled nearinfrared organolead halide perovskite solar cells. Angewandte International Edition Chemie 2016;128(13):4352-4356. DOI: 10.1002/anie.201600702.

[129] Zhou D, Liu D, Jin J, Chen X, Xu W, Yin Z et al. Semiconductor plasmon-sensitized broadband upconversion and its enhancement effect on the power conversion efficiency of perovskite solar cells. Journal of Materials Chemistry A 2017;5(32) 16559-16567. DOI: 10.1039/C7TA04943A.

[130] Straus DB, Kagan CR. Electrons, excitons, and phonons in two-dimensional hybrid perovskites: connecting structural, optical, and electronic properties. The journal of physical chemistry letters 2018;9(6) 1434-1447. DOI: 10.1021/acs.jpclett.8b00201.

[131] Katan C, Mercier N, Even J. Quantum and dielectric confinement effects in lower-dimensional hybrid perovskite semiconductors. Chemical

reviews 2019;119(5) 3140-3192. DOI: 10.1021/acs.chemrev.8b00417.

[132] Zhang L, Liu Y, Yang Z, Liu SF. Two dimensional metal halide perovskites: Promising candidates for light-emitting diodes. Journal of Energy Chemistry 2019;37 97-110. DOI: 10.1016/j.jechem.2018.12.005.

[133] Sutherland BR, Sargent EH. Perovskite photonic sources. Nature Photonics 2016;10(5) 295-305. DOI: 10.1038/nphoton.2016.62. DOI: 10.1016/j.jechem.2018.12.005.

[134] Kim YH, Cho H, Lee TW. Metal halide perovskite light emitters. Proceedings of the National Academy of Sciences. 2016 Oct 18;113(42):11694-702. DOI: 10.1073/pnas.1607471113.

[135] Kim YH, Cho H, Heo JH, Kim TS, Myoung N, Lee CL et al. Multicolored organic/inorganic hybrid perovskite light-emitting diodes. Advanced materials 2015;27(7) 1248-1254. DOI: 10.1002/adma.201403751.

[136] You P, Li G, Tang G, Cao J, Yan F. Ultrafast laser-annealing of perovskite films for efficient perovskite solar cells. Energy & Environmental Science 2020;13(4) 1187-1196. DOI: 10.1039/C9EE02324K.

[137] Wang H, Cao S, Yang B, Li H, Wang M, Hu X et al. NH_4Cl-Modified ZnO for High-Performance $CsPbIBr_2$ Perovskite Solar Cells via Low-Temperature Process. Solar Rrl 2020;4(1) 1900363. DOI: 10.1002/solr.201900363.

[138] Li Y, Hoye RL, Gao HH, Yan L, Zhang X, Zhou Y et al. Over 20% Efficiency in Methylammonium Lead Iodide Perovskite Solar Cells with Enhanced Stability via "in Situ Solidification" of the TiO_2 Compact Layer. ACS Applied Materials & Interfaces 2020;12(6) 7135-7143. DOI: 10.1021/acsami.9b19153.

[139] Oz S, Jena AK, Kulkarni A, Mouri K, Yokoyama T, Takei I et al. Lead (II) Propionate Additive and a Dopant-Free Polymer Hole Transport Material for $CsPbI_2Br$ Perovskite Solar Cells. ACS Energy Letters 2020;5(4) 1292-1299. DOI: 10.1021/acsenergylett.0c00244.

[140] Fu S, Zhang W, Li X, Wan L, Wu Y, Chen L et al. Dual-Protection Strategy for High-Efficiency and Stable $CsPbI_2Br$ Inorganic Perovskite Solar Cells. ACS Energy Letters 2020;5(2) 676-684. DOI: 10.1021/acsenergylett.9b02716.

[141] Li C, Pan Y, Hu J, Qiu S, Zhang C, Yang Y et al. Vertically Aligned 2D/3D Pb–Sn Perovskites with Enhanced Charge Extraction and Suppressed Phase Segregation for Efficient Printable Solar Cells. ACS Energy Letters 2020;5(5) 1386-1395. DOI: 10.1021/acsenergylett.0c00634.

[142] Wang D, Li W, Du Z, Li G, Sun W, Wu J et al. Highly efficient $CsPbBr_3$ planar perovskite solar cells via additive engineering with NH_4SCN. ACS Applied Materials & Interfaces 2020;12(9) 10579-10587. DOI: 10.1021/acsami.9b23384.